

Towards a universal set of topologically protected gates for quantum computation with Pfaffian qubits

Lachezar S. Georgiev

*Institute for Nuclear Research and Nuclear Energy
Tsarigradsko Chaussee 72, 1784 Sofia, BULGARIA*

Abstract

We review the topological quantum computation scheme of Das Sarma et al. from the perspective of the conformal field theory for the two-dimensional critical Ising model. This scheme originally used the *monodromy* properties of the non-Abelian excitations in the Pfaffian quantum Hall state to construct elementary qubits and execute logical NOT on them. We extend the scheme of Das Sarma et al. by exploiting the explicit *braiding* transformations for the Pfaffian wave functions containing 4 and 6 quasiholes to implement, for the first time in this context, the single-qubit Hadamard and phase gates and the two-qubit Controlled-NOT gate over Pfaffian qubits in a topologically protected way. In more detail, we explicitly construct the unitary representations of the braid groups \mathcal{B}_4 , \mathcal{B}_6 and \mathcal{B}_8 and use the elementary braid matrices to implement one-, two- and three-qubit gates. We also propose to construct a topologically protected Toffoli gate, in terms of a braid-group based Controlled-Controlled-Z gate precursor. Finally we discuss some difficulties arising in the embedding of the Clifford gates and address several important questions about topological quantum computation in general.

Key words: Topological quantum computation, Conformal field theory, Non-Abelian statistics

PACS: 11.25.Hf, 71.10.Pm, 73.40.Hm

1 Introduction

In contrast to the three dimensional world, where we could only find bosons and fermions, the statistics of localized objects in two dimensions turned out to be much richer, and includes fractional or anyonic statistics [1]. In the simplest case

Email address: lgeorg@inrne.bas.bg (Lachezar S. Georgiev).

of Abelian fractional statistics the counter-clockwise exchange of two anyons multiplies the many-body state by the statistical phase $\exp(i\theta)$, where θ/π might be a fractional number. The most important distinction between anyons on one side and bosons or fermions on the other is that the clockwise and counter-clockwise exchanges are significantly different so that the many-body wave functions belong to the representations spaces not of the permutation group but of the braid group [1,2]. When the dimension of the braid-group representation is bigger than 1 the corresponding (quasi)particles are called plektons [3,4,5], or non-Abelian anyons, and the exchange of two such anyons results in a non-trivial statistical matrix acting over degenerate space of many-body states. As the matrices representing different exchanges do not commute in general, this kind of quasiparticle statistics is called non-Abelian.

The most promising two-dimensional system, in which non-Abelian statistics may eventually be observed seems to be the fractional quantum Hall (FQH) state in the second Landau level with filling factor $v = 5/2$, which is now routinely observed in ultra high-mobility samples [6,7]. Convincing analytical [8,9] and numerical [10,11] evidence suggest that this state is most likely in the universality class of the Pfaffian FQH state constructed by Moore and Read [12] using correlation functions of certain operators in an appropriate $1 + 1$ dimensional conformal field theory (CFT) [13] including the Ising model [12,14]. Experimental tests of fractional statistics appear to be much more difficult than those which confirmed the fractional electric charge [15] of the FQH quasiparticles. However, it turns out that consequences of the presence of non-Abelian excitations might in fact be easier to observe than the Abelian fractional statistics itself despite the structural complications. In recent theoretical work interesting proposals for detection of the non-Abelian statistics of the quasiparticles in the $v = 5/2$ FQH state [16,17,18,19] and in the $v = 12/5$ FQH state [20,21], which is expected to be in the universality class of the $k = 3$ parafermion Hall state [22,23], have been made.

It is quite remarkable that in addition to its fundamental significance, the non-Abelian quantum statistics might become practically important for quantum computation [24]. Although the ideas behind quantum information processing are simply based on the well-established fundamental postulates of the quantum theory, its exponentially growing computational power could not have been exploited so far due to the unavoidable effects of quantum noise and decoherence as a result of interaction of the qubits with their environment. Even the quantum error-correcting algorithms [24], which allow to use operations containing certain level of errors, could not help creating a quantum computer with more than a few qubits. In this context recently appeared the idea of *topological quantum computation* (TQC) [25,26,27]. Because the interactions leading to decoherence are presumably local we can try to avoid them by encoding quantum information non-locally, using some global e.g., topological characteristics of the system. This *topological protection of qubit operations* means that quantum information is inaccessible to local interactions, because they cannot distinguish between the computational basis states and

hence cannot lead to decoherence and noise [25,27,28,29]. That is why topological gates are believed to be exact operations, which might potentially allow for the topologically protected quantum computation.

The FQH liquid is a perfect candidate for TQC because it possesses a number of topological properties which are universal, i.e., robust against the variations of the interactions details, and could be successfully described by rational conformal field (RCFT) theories [30,31,32], which capture the universality classes of the FQH edge excitations (see also [33] and Refs. therein). The main idea is to use the braiding matrices [3,4,27] corresponding to the exchanges of FQH quasiparticles, acting over a degenerate set of topological many-body states, to implement arbitrary unitary transformations [25,26,27,34]. Because the single qubit space is two-dimensional, we need degenerate spaces of quasiparticle correlation functions with dimension at least 2. While the Abelian FQH quasiparticles have degenerate spaces on non-trivial manifolds such as torus [25,35], such constructions are not appropriate for experimental realization in planar systems, such as the FQH liquids. Alternatively, by Abelian anyons, one could realize in the plane only diagonal gates, such as Controlled-phase gates [36] but cannot implement non-diagonal gates such as the Hadamard gate. In contrast, the non-Abelian FQH quasiparticles by definition have degenerate spaces even in planar geometry, which explains why the non-Abelian anyons might be more appropriate for TQC. The only residual source of noise and decoherence is due to thermally activated quasiparticle–quasihole pairs, which might execute unwanted braidings. Fortunately, these processes are exponentially suppressed at low temperature by the bulk energy gap, which leads to astronomical precision of quantum information processing.

In a recent paper [28] Das Sarma et al. proposed to use the expected non-Abelian statistics of the quasiparticles in the Pfaffian FQH state to construct an elementary qubit and execute a logical NOT gate on it. The NOT-gate construction is very important for quantum computation because it underlies both the construction of the single-qubit gates and of the Controlled-NOT (CNOT) gate [24]. However the NOT gate is certainly not sufficient for universal computation, though it is reversible, because the universal classical gate, NAND/NOT, built from NOT is irreversible [37], while all quantum gates must be reversible. Therefore, in the TQC scheme of Das Sarma et al., we need to implement the CNOT gate (or reversible XOR), which plays a central role in the universal quantum computer [24,37].

The FQH state at $\nu = 5/2$ has one big advantage with respect to TQC—it is the most stable state, i.e., the one with the highest bulk energy gap, among all FQH states in which non-Abelian quasiparticle statistics is expected to be realized. Recent measurements of the energy gap [6,7] suggest that ratio noise/signal is expected to be of the order of 10^{-30} or even lower, which is an unprecedented number in the quantum computation field and might potentially allow for the construction of a truly scalable quantum computation platform. On the other hand, one serious drawback is that the quasiparticles braiding matrices cannot be used alone for uni-

versal quantum computation because, as we shall see later, the representation of the braid group turns out to be finite. This has to be compared with the state at $v = 12/5$, whose braiding matrices are expected to be universal, but whose energy gap is an order of magnitude lower than the $v = 5/2$ one, which increases dramatically the noise/signal ratio.

In this paper we extend the TQC scheme of Das Sarma et al. [28], which was originally based on monodromy transformations of the Pfaffian wave functions, in such a way to construct by braiding the single-qubit Hadamard and phase gates as well as the two-qubit Controlled-Z and Controlled-NOT gates. These constructions are naturally topologically protected. In addition we investigate some possibilities for topologically protected realization of the three-qubit Toffoli gate.

Summary of results: we review in Sect. 2 the TQC scheme of Das Sarma et al. and introduce in Sect. 2.4 the 4-quasihole wave functions of Ref. [28] which we shall use to derive the elementary exchange matrices that will represent single-qubit gates. In Sect. 3 we consider in more detail the read-out transformation for the qubit of Ref. [28] by using the analytic properties of the 4-quasiholes states. We prove in Sect. 3.3 the orthogonality of the 4-quasiholes states forming the computational basis, which is very important for their quantum distinguishability. Deriving explicitly in Sect. 6 the exchange matrices for the 4-quasiholes states we construct in Sect. 8.3 all single-qubit gates, except for the $\pi/8$ gate, completely in terms of quasihole braiding. Then, in Sect. 8 we propose a natural two-qubit construction in terms of 6-quasiholes states and obtain explicitly the exchange matrices for these states. In Sects. 8.2 and 8.4 we implement the Controlled-Z and Controlled-NOT gates entirely in terms of 6-quasiholes braidings. To the best of the author's knowledge this is the first explicit construction of these gates in the Pfaffian state, which is exact and topologically protected. We also construct in Sects. 8.6 and 8.7 the Bravyi–Kitaev two-qubit gate g_3 and the non-demolition charge measurement gate, respectively, in terms of 6-quasiholes braidings. While the above gates are not sufficient for universal quantum computation they are known to form a Clifford group [38,35], which plays an extremely important role in error-correcting algorithms and, in particular could be efficiently used in such applications as quantum teleportation and super-dense coding [24]. Moreover, if the Clifford group is supplemented by the so-called magic states or noisy ancillas that could already be used for universal quantum computation [38]. In addition to the Clifford-group gates, instead of using the $\pi/8$ gate, we propose in Sect. 9 to implement in a topologically protected way the Toffoli gate in terms of the CNOT and the Controlled-S gate, or by a braid-group based Controlled-Controlled-Z gate precursor, which would actually form a universal set of topological protected gates realized with Pfaffian qubits. It appears that there is an additional topological entanglement in the three-qubit systems defined by 8 Pfaffian quasiholes, which leads to complications in the embedding of the one- and two-qubit gates into systems with three or more qubits. This phenomenon seems to be common for all topological quantum computation schemes based on the braid matrices of the non-Abelian FQH anyons.

2 The TQC scheme of Das Sarma et al.

The main idea of Ref. [28,29] is to use the wave functions of the Pfaffian FQH state with 4 quasiholes to form an elementary qubit. Then quantum gates can be executed by braiding some of the quasiholes (i.e., by counter-clockwise exchanges of quasiholes) leading to unitary transformations in the qubit space. When the positions of the quasiholes are fixed these wave functions form a 2-dimensional space which could be used as the single-qubit space. In general, the wave functions containing $2n$ quasiholes with fixed positions form a linear space with dimension 2^{n-1} [39]. The main reason for the exponential increase of the space dimension is the non-Abelian statistics of the quasiholes, i.e, when two quasiholes are fused together (taken to the same point in the coordinate plane) the result contains more than one quasiparticle due to the chiral Ising model fusion rule [12]

$$\sigma \times \sigma = \mathbb{I} + \psi. \quad (1)$$

The exponential degeneracy of the $2n$ quasiholes spaces can be alternatively understood by interpreting the Pfaffian state as a p -wave superconductor of composite fermions [8], where the non-Abelian quasiholes are represented by half-quantum vortices, and their non-Abelian statistics follows from the existence of Majorana zero-modes in the vortex cores obtained as solutions of the Bogolubov-de Gennes equations [8,9,40].

One way to keep the positions of the quasiholes fixed is to introduce antidots [41] (lithographically defined potential hills expelling the FQH fluid and creating a “hole” or “island” inside it) in the FQH liquid and localize the quasiholes there as shown on Fig. 1. The positions of the quasiholes are denoted by η_a , where $a = 1, \dots, 4$, and we assume that the quasiholes with coordinates η_1 and η_2 form our qubit, while η_3 and η_4 (not shown explicitly on Fig. 1) are used to measure and manipulate the qubit’s state [28,42].

2.1 State of the qubit and its initialization

In order to have a real TQC scheme we need to specialize the computational basis $\{|0\rangle, |1\rangle\}$. The definition of these states is closely related to the way we could possibly measure them and to the way we prepare the system in a certain state. That is why we shall start by saying how we can initialize the qubit and measure it.

To initialize the qubit we put charge $1/2$ on antidot 1 [28]. This can be done by adding one quantum h/e of magnetic flux in the vicinity of antidot 1 (e.g., by a solenoid piercing the antidot). A detailed analysis of the tunneling situation in the stable strong-coupling regime in a Pfaffian antidot with Aharonov–Bohm flux can

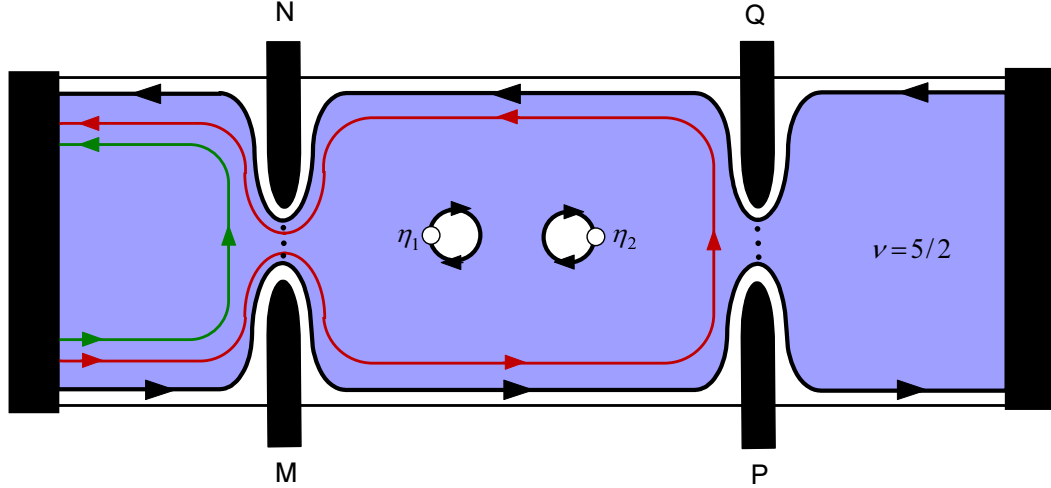


Fig. 1. (Color online). A $\nu = 5/2$ Hall bar with two antidots, on which the quasiholes (denoted symbolically by small empty circles) with coordinates η_1 and η_2 comprising the qubit are localized, and 4 front gates, M, N, P and Q creating tunneling constrictions. Black arrows depict the edge states, while the green and red arrows denote two alternative tunneling channels, a direct one and such enclosing the two antidots.

be found in Ref. [18]. The FQH liquid containing the antidot responds by localizing a charged excitation on the antidot border carrying one flux quantum. Because of the fundamental FQH effect relation between the magnetic flux and electric charge¹

$$Q_{\text{el}} = \nu \Phi, \quad \nu = \frac{1}{2}$$

the charge of such an excitation is $1/2$. There are only two allowed charge $1/2$ excitations of the Pfaffian FQH state which could be localized on the antidot: in the notation of Refs. [33,18] these are represented by the field operators

$$:e^{i\frac{1}{\sqrt{2}}\phi(z)}: \quad \text{and} \quad \psi(z):e^{i\frac{1}{\sqrt{2}}\phi(z)}:, \quad \Phi = 1, \quad Q_{\text{el}} = 1/2, \quad (2)$$

where $\psi(z)$ is the Ising model Majorana fermion and the vertex exponent of the normalized boson field $\phi(z)$ represents the $u(1)$ part of the excitation. Now we can envision the following computational basis

$$\begin{aligned} |0\rangle &\longleftrightarrow \text{ if the charge } 1/2 \text{ state is } :e^{i\frac{1}{\sqrt{2}}\phi(z)}: \\ |1\rangle &\longleftrightarrow \text{ if the charge } 1/2 \text{ state is } \psi(z):e^{i\frac{1}{\sqrt{2}}\phi(z)}:, \end{aligned} \quad (3)$$

¹ as usual we consider only the fractional part of the filling factor $\nu = 2 + 1/2$ corresponding to the top-most Landau level

or, in other words, the state of the qubit is $|0\rangle$ if the Majorana fermion is not occupied and $|1\rangle$ if it is occupied. Note that the states corresponding to the fields in Eq. (2) cannot form coherent superpositions because they belong to different superselection sectors inside the Naveu–Schwarz sector (when the flux threading antidot 1 is one quantum in the experimental setup), which correspond to their different fermion parity.

In Table 1 we give for convenience the list of the 6 topologically inequivalent sectors (quasiparticles) for the Pfaffian FQH state. Note that the topological sectors in which the chiral fermion parity is well-defined contain quasiparticles with both positive and negative parities because they can be obtained from each other by adding an electron. The quasiparticle spectrum is obtained from the chiral partition functions of the corresponding topological sectors, see Refs. [33,18] for more details.

Table 1

Topologically inequivalent quasiparticles in the Pfaffian FQH state and their quantum numbers: electric charge Q , neutral-sector chiral fermion parity γ_F , conformal dimension Δ and quantum statistics $\theta/\pi = 2\Delta \bmod 2$

Particles in the same Topological Sector	Fields	Charge Q	Parity γ_F	CFT dim. Δ	Quant. stat. θ/π
vacuum	\mathbb{I}	0	+	0	0
hole/electron	$e^{\pm i\sqrt{2}\phi}\psi$	± 1	–	$3/2$	1
quasihole (vortex)	$e^{i\frac{1}{2\sqrt{2}}\phi}\sigma$	$1/4$	undefined	$1/8$	$1/4$
quasiparticle	$e^{-i\frac{1}{2\sqrt{2}}\phi}\sigma$	$-1/4$	undefined	$1/8$	$1/4$
+1 flux	$e^{i\frac{1}{\sqrt{2}}\phi}$	$1/2$	+	$1/4$	$1/2$
–1 flux \times Majorana	$e^{-i\frac{1}{\sqrt{2}}\phi}\psi$	$-1/2$	–	$3/4$	$-1/2$
–1 flux	$e^{-i\frac{1}{\sqrt{2}}\phi}$	$-1/2$	+	$1/4$	$1/2$
+1 flux \times Majorana	$e^{i\frac{1}{\sqrt{2}}\phi}\psi$	$1/2$	–	$3/4$	$-1/2$
+2 flux (κ -boson)	$e^{i\sqrt{2}\phi}$	1	+	1	0
Majorana fermion	ψ	0	–	$1/2$	1

2.2 Measurement of the qubit state

It was one of the bright ideas of Ref. [28] to use the electronic Mach–Zehnder interferometry [43,44,19] to determine the state of the qubit. More precisely, let us try to measure the diagonal conductance, σ_{xx} , which is proportional to the probability for a charged particle to enter the lower edge of the Hall bar in Fig. 1 and to exit

in and out of the upper edge. Because of the constrictions created by the front gates M and N, P and Q, there are two alternative channels for a charged quasiparticle entering from the lower edge to exit from the upper one: one is to tunnel between the front gates M and N and the other is to tunnel between P and Q. Therefore, to leading order in the tunneling amplitudes t_{MN} and t_{PQ} , which are assumed to be very small, the diagonal conductance would be proportional to the interference of the two amplitudes [28]. Consider, for example the interference of the two tunneling processes if the charge 1/2 on antidot 1 does not contain Majorana fermion. Then the amplitude for tunneling between P and Q must be multiplied by the Aharonov–Bohm phase for the non-Abelian quasi-hole which when tunneling between P and Q actually encircles the charge 1/2 state on antidot 1, i.e.,

$$e^{2\pi i \Phi Q_{\text{el}}} = e^{i\frac{\pi}{2}} = i, \quad (4)$$

because a quasiparticle with charge $Q_{\text{el}} = 1/4$ encircles magnetic flux $\Phi = 1$. Therefore, the diagonal conductance, which is proportional to the modulus-square of the amplitude, reads

$$\sigma_{xx}^{(0)} \propto |t_{MN} + i t_{PQ}|^2. \quad (5)$$

If instead, the state of the qubit is $|1\rangle$, i.e., there is a Majorana fermion on antidot 1, then in addition to the Aharonov–Bohm phase (4) there would be a minus sign coming from the fact that the Ising model σ field is transported around the Majorana fermion. To see, in the CFT language, why this minus sign appears, we consider the operator-product-expansion

$$\sigma(z)\psi(0) \underset{z \rightarrow 0}{\sim} \frac{\sigma(0)}{\sqrt{2z}} \quad \text{so that} \quad \sigma(z)\psi(0) \rightarrow -\sigma(z)\psi(0) \quad \text{when} \quad z \rightarrow e^{2\pi i}z,$$

i.e., when σ is transported adiabatically around ψ . Thus, the diagonal conductance measurement in the state $|1\rangle$ gives

$$\sigma_{xx}^{(1)} \propto |t_{MN} - i t_{PQ}|^2. \quad (6)$$

Note that the two different interference patterns, Eqs. (5) and (6) of the diagonal conductance are very well distinguished experimentally due to the high visibility of the Mach–Zehnder interferometry [43].

2.3 Splitting the 1/2 charge: finalizing the qubit

Despite that we can efficiently measure the two states in the computational basis this is still not sufficient for quantum computation. The reason is that we need

to form coherent superpositions of the states $|0\rangle$ and $|1\rangle$ which is not allowed for the charge 1/2 states (3) due to the fermion parity superselection rule. In order to circumvent this difficulty Das Sarma et al. have made another interesting proposal [28]: to split the charge 1/2 state into $1/4 \times 1/4$ state by transferring one charge 1/4 from antidot 1 to antidot 2. This is indeed possible, if one applies voltage between the two antidots, because the most relevant quasiparticle for tunneling through the bulk of the Pfaffian FQH liquid carries charge 1/4. This quasiparticle is non-Abelian and contains a σ field from the Ising model because there is no other charge 1/4 quasiparticle and the non-Abelian one has the minimal CFT dimension [12,39,33]. Now the state on antidots 1 and 2 is equivalent to $\sigma(\eta_1)\sigma(\eta_2)$ which together with the quasiholes at η_3 and η_4 correspond to a 4-quasihole wave function, which belongs to a two-dimensional space as discussed in the beginning of Sect. 2.

While the charge 1/2 states (3) cannot form coherent superpositions, because they belong to different superselection sectors, for the 4 quasiholes configurations we can consider the superposition of the states obtained by splitting of the vacuum in two different ways, namely

$$\begin{aligned} \mathbb{I} &\rightarrow \mathbb{I} \times \mathbb{I} \rightarrow (\sigma \times \sigma) \times (\sigma \times \sigma) \\ \mathbb{I} &\rightarrow \psi \times \psi \rightarrow (\sigma \times \sigma) \times (\sigma \times \sigma), \end{aligned} \tag{7}$$

because the two 4-quasihole states now belong to the same superselection sectors.

One natural question arises in this charge splitting procedure: *does the state of the qubit remain the same in the process of transferring one charge 1/4 from antidot 1 to antidot 2 or it changes?* Or, even, more philosophically: *does the system with 4 σ fields has something in common with the computational basis of our charge 1/2 state plus 2 additional σ fields, or it is completely different?*

The original idea of Ref. [28] was that the state of the qubit does not change during the splitting procedure because the pairs of quasiholes in the Pfaffian state share a pair of Majorana fermions zero modes, $(\psi_0, \bar{\psi}_0)$, whose combined (left- plus right- moving) fermion parity is supposed to be conserved. That's why the readout should give the same results as before splitting unless some Majorana fermions could tunnel from the edge or from another antidot, however, these processes are exponentially suppressed because the quasiholes are supposed to be well separated and far from the edges.

In Sect. 3 we shall explicitly derive the readout results for the 4-quasiholes wave functions and will find conditions under which this is in agreement with Ref. [28].

2.4 Four-quasiholes wave functions

As we shall see in Sect. 3, the topological phase, which determines the conductance interference pattern, can be obtained from the monodromy matrices appearing in the adiabatic transport of some quasiholes around others, so that we need the wave functions explicitly. The wave function for even number N of holes (or electrons) at positions z_1, \dots, z_N containing 4 quasiholes at positions η_1, \dots, η_4 , can be realized as a correlation function

$$\Psi_{4\text{qh}}(\eta_1, \eta_2, \eta_3, \eta_4; \{z_i\}) = \langle \psi_{\text{qh}}(\eta_1) \psi_{\text{qh}}(\eta_2) \psi_{\text{qh}}(\eta_3) \psi_{\text{qh}}(\eta_4) \prod_{i=1}^N \psi_{\text{hole}}(z_i) \rangle$$

of the field operators corresponding to creation of holes and quasiholes

$$\psi_{\text{hole}}(z) = \psi(z) : e^{i\sqrt{2}\phi(z)} : \quad \text{and} \quad \psi_{\text{qh}}(\eta) = \sigma(\eta) : e^{i\frac{1}{2\sqrt{2}}\phi(\eta)} :; \quad (8)$$

respectively, where $\sigma(\eta)$ is the chiral spin field in the Ising model of dimension $1/16$ and $\psi(z)$ is the right-moving Majorana fermion in the chiral Ising model. It can be expressed as

$$\begin{aligned} \Psi_{4\text{qh}}(\eta_1, \eta_2, \eta_3, \eta_4; z_1, \dots, z_N) = & \left\langle \sigma(\eta_1) \sigma(\eta_2) \sigma(\eta_3) \sigma(\eta_4) \prod_{j=1}^N \psi(z_j) \right\rangle \times \\ & \prod_{1 \leq a < b \leq 4} \eta_{ab}^{\frac{1}{8}} \prod_{i=1}^N \sqrt{(z_i - \eta_1)(z_i - \eta_2)(z_i - \eta_3)(z_i - \eta_4)} \prod_{1 \leq i < j \leq N} z_{ij}^2, \end{aligned} \quad (9)$$

where the average sign $\langle \dots \rangle$ now represents the vacuum expectation value in the chiral Ising model and the last three product factors in Eq. (9) come from the $u(1)$ components of the holes $: \exp(i\sqrt{2}\phi(z)) :$ and of the quasiholes $: \exp(i\phi(z)/2\sqrt{2}) :$. We used here the notation $\eta_{ab} \equiv \eta_a - \eta_b$ for $a \neq b$ and $z_{ij} = z_i - z_j$ for $i \neq j$.

One important detail is that the chiral field $\sigma(\eta)$ does not have a definite fermion parity because of the non-Abelian fusion rule (1) which mixes states with different fermion parities. Nevertheless it would be convenient to introduce two chiral fields σ_{\pm} of dimension $\Delta_{\pm} = 1/16$ and opposite parities [33]

$$\gamma_F \sigma_{\pm}(\eta) \gamma_F = \pm \sigma_{\pm}(\eta), \quad (10)$$

in terms of which the non-Abelian fusion rule (1) necessarily splits into two Abelian channels

$$\sigma_{\pm} \times \sigma_{\pm} = \mathbb{I}, \quad \sigma_{\pm} \times \sigma_{\mp} = \psi. \quad (11)$$

The σ filed entering Eq. (9) is then identified with

$$\sigma(\eta) = \frac{\sigma_+(\eta) + \sigma_-(\eta)}{\sqrt{2}}. \quad (12)$$

In order to obtain the 4-qh wave function (9) we carefully repeat the arguments of Ref. [39] in which the chiral many-body wave functions of the Pfaffian state are obtained by bosonization techniques from the $c = 1$ complex Ising model. The final result is

$$\Psi_{4\text{qh}}(\eta_1, \eta_2, \eta_3, \eta_4; z_1, \dots, z_N) = \Psi_{4\text{qh}}^{(0)} + \Psi_{4\text{qh}}^{(1)}, \quad (13)$$

where we have used the notation of Refs. [28,39] ($\Psi_{4\text{qh}}^{(0)} \equiv |0\rangle$, $\Psi_{4\text{qh}}^{(1)} \equiv |1\rangle$ would be our computational basis in the 4-qh wave function's space)

$$\Psi_{4\text{qh}}^{(0,1)} = \frac{(\eta_{13}\eta_{24})^{\frac{1}{4}}}{\sqrt{1 \pm \sqrt{x}}} (\Psi_{(13)(24)} \pm \sqrt{x}\Psi_{(14)(23)}) \quad (14)$$

with x being a CFT invariant crossratio [13]

$$x = \frac{\eta_{14}\eta_{23}}{\eta_{13}\eta_{24}} \quad \text{and} \quad (\eta_{ab} = \eta_a - \eta_b), \quad (15)$$

$$\begin{aligned} \Psi_{(ab)(cd)} &= \text{Pf} \left(\frac{(z_i - \eta_a)(z_i - \eta_b)(z_j - \eta_c)(z_j - \eta_d) + (i \leftrightarrow j)}{z_i - z_j} \right) \times \\ &\times \prod_{1 \leq i < j \leq N} (z_i - z_j)^2, \end{aligned}$$

where $\{a, b, c, d\}$ is a permutation of $\{1, 2, 3, 4\}$ satisfying $a < b$ and $c < d$. The Pfaffian of an anti-symmetric matrix M_{ij} of even dimension N is defined as

$$\text{Pf}(M_{ij}) = \frac{1}{2^{N/2}((N/2)!)^2} \sum_{\sigma \in S_N} \text{sign}(\sigma) \prod_{k=1}^{N/2} M_{\sigma(2k-1)\sigma(2k)}.$$

It is worth stressing that the space of the 4-quasihole wave functions for fixed positions of the quasiholes is two-dimensional. The second independent wave function could be obtained from the first one, Eq. (13), by transporting η_3 around η_4 (i.e., $\eta_{34} \rightarrow e^{2\pi i} \eta_{34}$) which transforms $\Psi_{4\text{qh}}^{(0)} \rightarrow \Psi_{4\text{qh}}^{(0)}$ and $\Psi_{4\text{qh}}^{(1)} \rightarrow -\Psi_{4\text{qh}}^{(1)}$ so that

$$\tilde{\Psi}_{4\text{qh}}(\eta_1, \eta_2, \eta_3, \eta_4; z_1, \dots, z_N) = \Psi_{4\text{qh}}^{(0)} - \Psi_{4\text{qh}}^{(1)}. \quad (16)$$

It appears, however, that in some situations, such as the qubit initialization of Ref. [28], the 4-qh wave function may be driven directly in the state $\Psi_{4\text{qh}}^{(0)}$ or $\Psi_{4\text{qh}}^{(1)}$.

3 Read-out in the TQC scheme of Das Sarma et al: the measurement of the 4-quasiholes qubit state

As we have seen in Sect. (2.2) the read-out of the qubit is performed by interference measurement of the diagonal conductance, for which we need the monodromies of the corresponding wave functions. In this section we shall compute the explicit monodromies of the 4-qh wave functions (14) as well as for (13) and (16). Then, in Sect. 4, we shall compute the corresponding monodromies for the two charge 1/2 states, which can be obtained by fusing quasiholes with coordinates η_1 and η_2 .

Assuming that our qubit is formed by the quasiholes with coordinates η_1 and η_2 we can interpret the quasiholes with coordinate η_3 tunneling either through M and N or through P and Q as generating the interference pattern in the longitudinal conductance, like in the non-Abelian Mach–Zehnder interferometer [44]. In more detail, if the third quasihole tunnels through M and N, as shown on Fig. 2, this

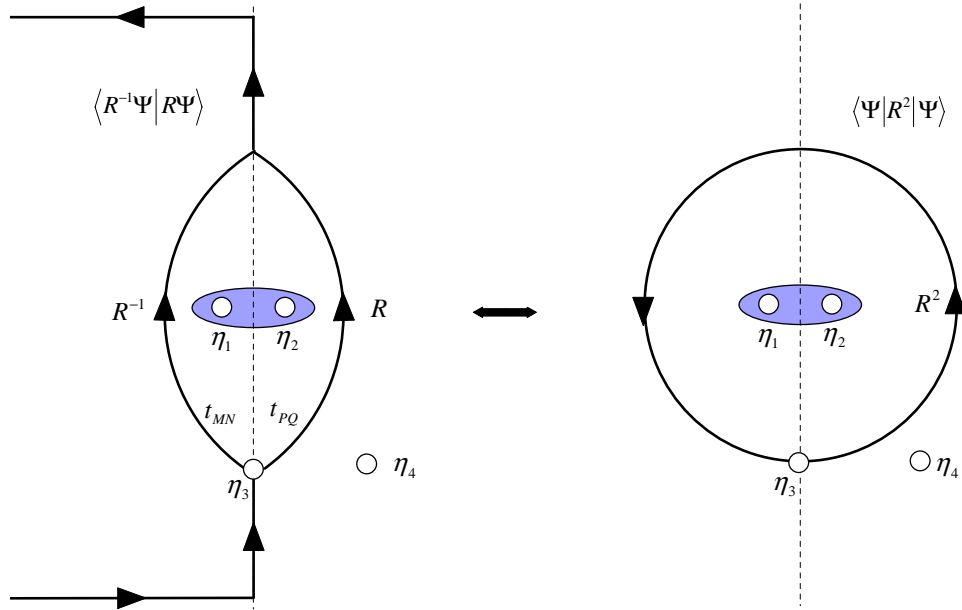


Fig. 2. Conductance interference term in the read-out procedure expressed by the braids R (corresponding to tunneling through P and Q), R^{-1} (corresponding to tunneling through M and N) and the monodromy R^2 .

could be interpreted as a clockwise braid of this quasi-hole with the qubit, while if it tunnels through P and Q this gives rise to a counter-clockwise braid (denoted below as R ; cf. Ref. [44]) so that the quantum amplitude for these two processes is (we

have absorbed all dynamical phase factors for the two paths in the corresponding amplitudes t_{MN} and t_{PQ})

$$|A\rangle = t_{MN} R^{-1} |(\eta_1, \eta_2), \eta_3, \eta_4\rangle + t_{PQ} R |(\eta_1, \eta_2), \eta_3, \eta_4\rangle$$

and the longitudinal conductance would be

$$\sigma_{xx} \propto \langle A|A\rangle = |t_{MN}|^2 + |t_{PQ}|^2 + 2\text{Re} (t_{MN}^* t_{PQ} \langle \Psi | R^2 | \Psi \rangle),$$

where $|\Psi\rangle = |(\eta_1, \eta_2), \eta_3, \eta_4\rangle$ is the 4-qh state in which the qubit is formed by the quasiholes with positions η_1 and η_2 , and we have used the unitarity of the braid operator R and R^2 is the corresponding monodromy operator. The operator R^2 is actually the operator which *takes the quasihole with coordinate η_3 around those with η_1 and η_2 in counter-clockwise direction*. Note that if we fuse the quasiholes forming the qubit, i.e., $\eta_1 \rightarrow \eta_2$, and the state is \mathbb{I} then the matrix element is $+i$, while if they fuse to ψ the matrix element is $-i$, which reproduce the interference results in Sect. 2.2. It is worth stressing that there is a remarkable relation between the expectation value of the monodromy operator R^2 , corresponding to the adiabatic transport of particle with label a around particle with label b , and the modular S matrix [13] associated with any rational CFT [20]:

$$\langle \Psi | R^2 | \Psi \rangle = \frac{S_{ab} S_{00}}{S_{0a} S_{0b}},$$

where the label 0 corresponds to the vacuum. Working with modular S matrices is very convenient because they are explicitly known for almost all rational CFT related to the FQH effect.

Thus we see that the read-out or measurement procedure for the 4-qh wave functions consists in taking the quasihole with coordinate η_3 around the qubit [28,42], i.e., around the two quasiholes with coordinates η_1 and η_2 .²

It is worth stressing that the 4-qh wave function basis (14) is very convenient from the point of view of the adiabatic transport because the functions $\Psi_{(ab)(cd)}$ have no Berry phases [39] so that the transport effects could be explicitly determined from the monodromies of the multivalued function

$$f(z) = \sqrt{1 \pm \sqrt{z}}, \quad z \in \mathbb{C},$$

entering the denominator in Eq. (14). Notice, however, that “taking η_3 around η_1

² Alternatively, as a matter of choice, one could use the quasihole with the coordinate η_4 to encircle the quasiholes localized on antidots 1 and 2, which would lead to the same results, however, we will stick here to the notation of Ref. [28]).

and η_2 ” in the functions (19) for $z = x$ with x defined in Eq. (15), which are simply proportional to the 4-point functions of the chiral spin field in the Ising model, is equivalent to the adiabatic transport of η_3 around η_4 alone. This is because the monodromy for the transport of η_3 around η_1 , η_2 and η_3 is trivial, as shown on Fig. 3, since the contour on the left can be contracted to a point (at infinity) without

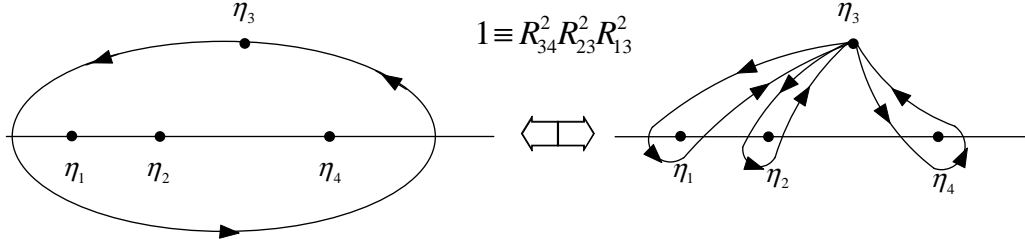


Fig. 3. The trivial monodromy of the 4-quasihole wave function, when one quasihole is transported around all others, allows to compute the read-out as taking η_3 around η_4 .

passing through any other singularity. Therefore it would be simpler to compute the read-out transformation of the functions (19) for $z = x$ by

$$R_{34}^2 : \quad \eta_{34} \rightarrow \eta'_{34} = \lim_{t \rightarrow 1_-} e^{2\pi i t} \eta_{34}, \quad t \in [0, 1). \quad (17)$$

The transformation (17) obviously preserves the absolute value of the crossratio

$$\tilde{x} \equiv \frac{\eta_{12} \eta_{34}}{\eta_{13} \eta_{24}} = 1 - x \quad \Leftrightarrow \quad x = 1 - \tilde{x}, \quad (18)$$

where x is defined in Eq. (15), because all other $\eta'_{ab} = \eta_{ab}$, i.e., the contour for transportation of \tilde{x} , corresponding to Eq. (17), is a circle with center at $\tilde{x} = 0$ and radius $|\tilde{x}|$. Therefore the result crucially depends on whether $|\tilde{x}|$ is bigger or smaller than 1. Thus we need to consider the behavior of the functions

$$f_{\pm}(\tilde{x}) = \sqrt{1 \pm \sqrt{1 - \tilde{x}}} \quad (19)$$

under the transformation (17). Yet, it is more convenient to first analyze Eq. (19) as a function of z and then just outline what happens when we change $z = 1 - \tilde{x}$.

The multivalued function (19) has two separate branching points: one is $z = 0$ which, if encircled by the continuation contour, would change the sign of the inner root, as can be seen from Eq. (A.2) in Appendix A, i.e.,

$$\sqrt{1 \pm \sqrt{z}} \rightarrow \sqrt{1 \mp \sqrt{z}}, \quad \text{for } z \rightarrow e^{2\pi i} z \quad \text{and} \quad |z| < 1.$$

However, the second function, corresponding to the minus sign under the square root in Eq. (19), has one more branching point at $z = 1$ which, if encircled in the process of the analytic continuation changes the sign of the outer root, i.e.,

$$\sqrt{1 \pm \sqrt{z}} \rightarrow \pm \sqrt{1 \pm \sqrt{z}}, \quad \text{for } (z-1) \rightarrow e^{2\pi i}(z-1) \text{ and } |z-1| < 1.$$

This can be easily seen from the Laurent-mode expansion for $|z-1| < 1$, by looking at Eq. (A.4) in Appendix A.

Now consider what happens when we change $z = 1 - \tilde{x}$. When $\tilde{x} \rightarrow e^{2\pi i t} \tilde{x}$, and t goes from 0 to 1, this transports \tilde{x} along a circle of radius $|\tilde{x}|$ and center at $\tilde{x} = 0$. Then $- \tilde{x}$ is transported along the same circle, though with a phase shift of π . Thus $z = 1 - \tilde{x}$ is transported along a circle of the same radius $|\tilde{x}|$, however translated to be centered at $z = 1$ as shown on Figures 4 and 5.

Therefore we need to consider both cases, $|\tilde{x}| < 1$ and $|\tilde{x}| > 1$, separately in more detail. Of course, one may consider other contours which are homotopic to that of Eq. (17) but do not preserve the absolute value of \tilde{x} . In that case the results would be the same as those obtained from Eq. (17), only the conditions on $|\tilde{x}|$ must be replaced by the homotopic condition whether these contours encircle both branching points $z = 0$ and $z = 1$ or only one of them.

3.1 The read-out for $|\tilde{x}| < 1$: take η_3 around η_4

According to our analysis, when $|\tilde{x}| < 1$, the read-out transformation (17) corresponds to transporting the crossratio (18) along a contour which encircles only the branching point at $z = 1$,

$$C_{\tilde{x}}^< = \{z = 1 - e^{2\pi i t} \tilde{x} \mid 0 \leq t \leq 1, \quad |\tilde{x}| < 1\}, \quad (20)$$

as shown in Fig. 4. We have introduced two branch-cuts for the function (19) like in Fig. 4. Because the 4-quasihole wave functions $\Psi_{(13)(24)}$ and $\Psi_{(14)(23)}$ have no branch-cuts in η_{ab} , they acquire no phase under the transformation (17), and the only phases come from the prefactor in Eq. (14) containing η_{ab} and x .

Since $|\tilde{x}| < 1$ and the transformation (17) transports \tilde{x} along the contour (20), which is shown on Fig. 4, this transformation only changes the outer-roots signs, i.e.,

$$R_{34}^2 \begin{pmatrix} \sqrt{1 + \sqrt{1 - \tilde{x}}} \\ \sqrt{1 - \sqrt{1 - \tilde{x}}} \end{pmatrix} = \begin{pmatrix} 1 & 0 \\ 0 & -1 \end{pmatrix} \begin{pmatrix} \sqrt{1 + \sqrt{1 - \tilde{x}}} \\ \sqrt{1 - \sqrt{1 - \tilde{x}}} \end{pmatrix}.$$

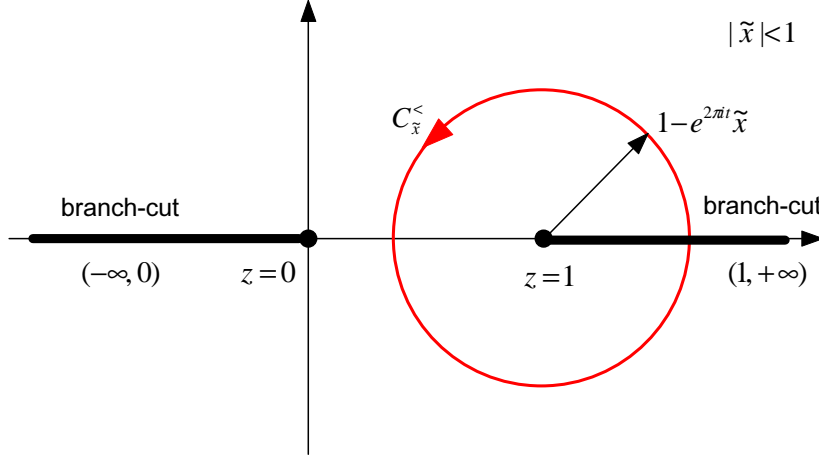


Fig. 4. The contour $C_{\tilde{x}}^<$ used for the analytic continuation of Eq. (19) when $|\tilde{x}| < 1$. As it encloses only the branching point at $z = 1$, going along this contour only changes the outer-root sign of $f_-(z)$.

In order to find the action of the transformation (17) in the basis $\{\Psi_{4\text{qh}}^{(0)}, \Psi_{4\text{qh}}^{(1)}\}$ we only have to add the phase coming from $\eta_{13}^{1/4}$ in Eq. (14) which is $e^{i\pi/2}$. Notice that we use “taking η_3 around η_4 ” as the readout prescription only for the functions (19) because these are the functions for which the total monodromy is trivial. For all other functions, including fractional powers of η_{ab} , we still use as the read-out “taking η_3 around η_1 and η_2 ”. Thus we obtain the read-out transformation as

$$U_{\text{read-out}}^{(|\tilde{x}| < 1)} \begin{pmatrix} \Psi_{4\text{qh}}^{(0)} \\ \Psi_{4\text{qh}}^{(1)} \end{pmatrix} = \begin{pmatrix} i & 0 \\ 0 & -i \end{pmatrix} \begin{pmatrix} \Psi_{4\text{qh}}^{(0)} \\ \Psi_{4\text{qh}}^{(1)} \end{pmatrix} \quad \text{for} \quad \left| \frac{\eta_{12}\eta_{34}}{\eta_{13}\eta_{24}} \right| < 1. \quad (21)$$

Notice that this “ $\pm i$ ”, on the diagonal of the matrix in Eq. (21), is exactly the topological phase that appears for the quasiparticles traveling along the contour passing through the front contacts P and Q, see Fig. 1, in the diagonal conductance measurement so that

$$\sigma_{xx}^{|\tilde{x}| < 1} \propto |t_{MN} \pm i t_{PQ}|^2, \quad \text{with “+” for } |0\rangle \text{ and “-” for } |1\rangle. \quad (22)$$

3.2 The case $|\tilde{x}| > 1$

Alternatively, if $|\tilde{x}| > 1$, then the read-out transformation (17) leads to transporting \tilde{x} along the following contour

$$C_{\tilde{x}}^> = \{z = 1 - e^{2\pi i t} \tilde{x} \mid 0 \leq t \leq 1, \quad |\tilde{x}| > 1\}, \quad (23)$$

which encircles both branching points at $z = 1$ and $z = 0$ as shown on Fig. 5. Therefore, the read-out transformations (17) would change the sign of the outer

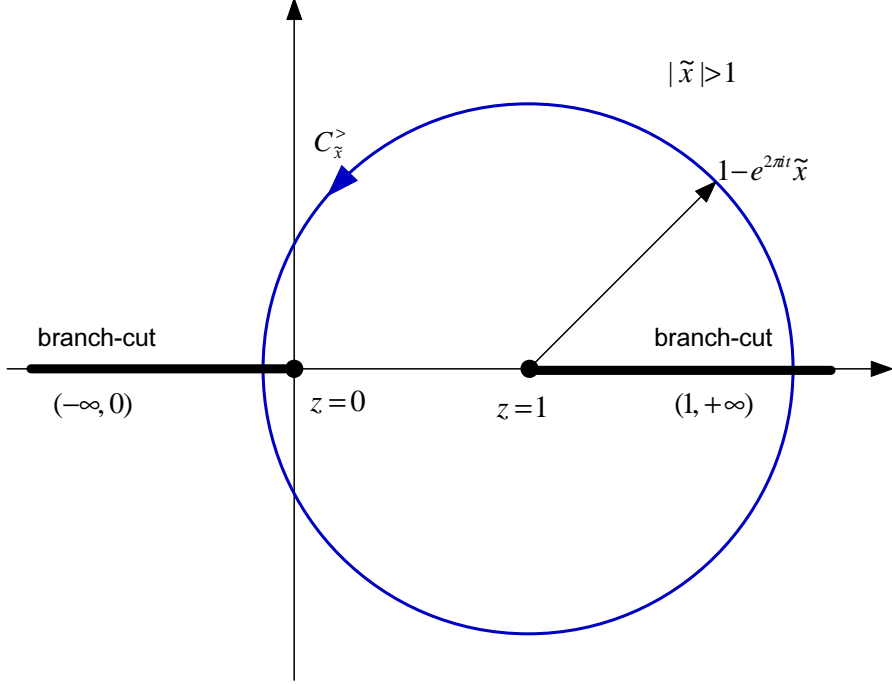


Fig. 5. The contour $C_{\tilde{x}}^>$ used for the analytic continuation of Eq. (19) when $|\tilde{x}| > 1$. Because it encloses both branching point at $z = 1$ and $z = 0$ going along this contour changes the outer-root sign whenever the inner one is “ $-$ ” and flips the inner-root sign of $f_{\pm}(z)$.

root whenever the inner sign is “ $-$ ” as well as would flip the inner-roots signs, i.e.,

$$R_{34}^2 \begin{pmatrix} \sqrt{1 + \sqrt{1 - \tilde{x}}} \\ \sqrt{1 - \sqrt{1 - \tilde{x}}} \end{pmatrix} = \begin{pmatrix} 0 & 1 \\ -1 & 0 \end{pmatrix} \begin{pmatrix} \sqrt{1 + \sqrt{1 - \tilde{x}}} \\ \sqrt{1 - \sqrt{1 - \tilde{x}}} \end{pmatrix}.$$

Adding again the Abelian phase $e^{i\pi/2}$, coming from $\eta_{13}^{1/4}$ in Eq. (14) we obtain the read-out transformation as

$$U_{\text{read-out}}^{(|\tilde{x}| > 1)} \begin{pmatrix} \Psi_{4\text{qh}}^{(0)} \\ \Psi_{4\text{qh}}^{(1)} \end{pmatrix} = \begin{pmatrix} 0 & i \\ -i & 0 \end{pmatrix} \begin{pmatrix} \Psi_{4\text{qh}}^{(0)} \\ \Psi_{4\text{qh}}^{(1)} \end{pmatrix} \quad \text{for} \quad \left| \frac{\eta_{12}\eta_{34}}{\eta_{13}\eta_{24}} \right| > 1. \quad (24)$$

Now the diagonal conductance measurement might be different from Eq. (22), as it crucially depends on the overlap between the states (14).

To conclude, let’s state the main result in this Section—the read-out procedure crucially depends on the absolute value of the crossratio (18). This has to be taken into account when real experiments with qubits realized in FQH systems at $v = 5/2$.

Using the CFT invariance of \tilde{x} , one can prove that the absolute value of the cross-ratio \tilde{x} depends on the absolute values of the quasiholes positions, i.e.,

$$|\tilde{x}| < 1 \Leftrightarrow |\eta_3| < |\eta_2|, \quad \text{while} \quad |\tilde{x}| > 1 \Leftrightarrow |\eta_3| > |\eta_2|.$$

3.3 Orthogonality of the 4-quasiholes wave function $\Psi_{4\text{qh}}^{(0,1)}$

One of the fundamental requirement in quantum theory is that the states $|0\rangle$, $|1\rangle$ are not only linearly independent but in fact orthogonal. Otherwise there exists no measurement that can reliably distinguish these states [24]. Here we will demonstrate that the 4-quasiholes states (14) are indeed orthogonal, at least for $|\tilde{x}| < 1$. This seems natural because, as we already know the Mach–Zehnder interferometer can distinguish the states (14), hence these states should be orthogonal. However, it is still worth verifying this directly if possible.

The point is that for $|\tilde{x}| < 1$ we have, according to Eq. (21), $U\Psi_{4\text{qh}}^{(0)} = i\Psi_{4\text{qh}}^{(0)}$ and $U\Psi_{4\text{qh}}^{(1)} = -i\Psi_{4\text{qh}}^{(1)}$, hence, $U^\dagger\Psi_{4\text{qh}}^{(0)} = -i\Psi_{4\text{qh}}^{(0)}$ and $U^\dagger\Psi_{4\text{qh}}^{(1)} = i\Psi_{4\text{qh}}^{(1)}$, where $U \equiv U_{\text{read-out}}$. In order to find the overlap $(\Psi_{4\text{qh}}^{(1)}, \Psi_{4\text{qh}}^{(0)})$ we first plug inside it the operator U and use the above relations, i.e., on one side we have

$$(\Psi_{4\text{qh}}^{(1)}, U\Psi_{4\text{qh}}^{(0)}) = i(\Psi_{4\text{qh}}^{(1)}, \Psi_{4\text{qh}}^{(0)}) \quad (25)$$

while, on the other side, using the definition of the Hermitean conjugation and the anti-linearity of the inner product with respect to its first argument, it is equal to

$$(U^\dagger\Psi_{4\text{qh}}^{(1)}, \Psi_{4\text{qh}}^{(0)}) = (i\Psi_{4\text{qh}}^{(1)}, \Psi_{4\text{qh}}^{(0)}) = -i(\Psi_{4\text{qh}}^{(1)}, \Psi_{4\text{qh}}^{(0)}). \quad (26)$$

Obviously the right-hand sides of Eqs. (25) and (26) could only be equal if

$$(\Psi_{4\text{qh}}^{(1)}, \Psi_{4\text{qh}}^{(0)}) = 0.$$

4 Measurement of the charge 1/2 state's wave function

As we have seen in Sect. 2.2 the state of the qubit before splitting $1/2 \rightarrow 1/4 \times 1/4$ is $|0\rangle$ if the Majorana fermion is absent or $|1\rangle$ if it is present in the charge-1/2 state. Using the fusion rules for two quasiholes (8)

$$\psi_{\text{qh}}(\eta_1)\psi_{\text{qh}}(\eta_2) \underset{\eta_1 \rightarrow \eta_2}{\simeq} \left(1 + \sqrt{\frac{\eta_{12}}{2}}\psi(\eta_2)\right) e^{i\frac{1}{\sqrt{2}}\phi(\eta_2)} \quad (27)$$

as well as the general fusion rule of vertex exponents

$$e^{i\lambda_a\phi(\eta_a)}e^{i\lambda_b\phi(\eta_b)} \underset{\eta_a \rightarrow \eta_b}{\simeq} \eta_{ab}^{\lambda_a\lambda_b} e^{i(\lambda_a+\lambda_b)\phi(\eta_b)}$$

we can deduce the form of the charge 1/2 wave functions from the 4-quasihole wave function (9) by taking $\eta_1 \rightarrow \eta_2$. Let us denote by Ψ_0 and Ψ_1 the result of fusing the two quasiholes ψ_{qh} to $e^{i\frac{\phi}{\sqrt{2}}}$ and $\psi e^{i\frac{\phi}{\sqrt{2}}}$ for $\eta_1 \rightarrow \eta_2$ as in Eq. (27), respectively, i.e.,

$$\begin{aligned} \Psi_0 &= \left\langle \sigma(\eta_3)\sigma(\eta_4) \prod_{i=1}^N \psi(z_i) \right\rangle \left\langle e^{i\frac{1}{\sqrt{2}}\phi(\eta_2)} e^{i\frac{1}{2\sqrt{2}}\phi(\eta_3)} e^{i\frac{1}{2\sqrt{2}}\phi(\eta_4)} \prod_{i=1}^N e^{i\sqrt{2}\phi(z_i)} \right\rangle \\ \Psi_1 &= \sqrt{\frac{\eta_{12}}{2}} \left\langle \psi(\eta_2)\sigma(\eta_3)\sigma(\eta_4) \prod_{i=1}^N \psi(z_i) \right\rangle \left\langle e^{i\frac{\phi(\eta_2)}{\sqrt{2}}} e^{i\frac{\phi(\eta_3)}{2\sqrt{2}}} e^{i\frac{\phi(\eta_4)}{2\sqrt{2}}} \prod_{i=1}^N e^{i\sqrt{2}\phi(z_i)} \right\rangle. \end{aligned} \quad (28)$$

Next we use the well-known formula

$$\left\langle \prod_{a=1}^N e^{i\lambda_a\phi(z_a)} \right\rangle = \prod_{a < b} (z_a - z_b)^{\lambda_a\lambda_b} \delta_{\lambda_1 + \dots + \lambda_N, 0}$$

to show that

$$\left\langle e^{i\frac{1}{\sqrt{2}}\phi(\eta_2)} e^{i\frac{1}{2\sqrt{2}}\phi(\eta_3)} e^{i\frac{1}{2\sqrt{2}}\phi(\eta_4)} \prod_{i=1}^N e^{i\sqrt{2}\phi(z_i)} \right\rangle = \eta_{23}^{1/4} \eta_{24}^{1/4} \eta_{34}^{1/8} \left\langle \begin{array}{c} \text{independent of} \\ \eta_{ab} \end{array} \right\rangle,$$

where the second expectation value on the right-hand side is independent of η_{ab} and therefore gives no contribution to monodromies. Similarly, noting in passing that the branch-cut structure of the wave functions with 2 or 3 quasiholes is determined by the corresponding 2-pt and 3-pt quasiholes functions, for even N we find

$$\left\langle \sigma(\eta_3)\sigma(\eta_4) \prod_{i=1}^N \psi(z_i) \right\rangle = \eta_{34}^{-1/8} \left\langle \begin{array}{c} \text{single-valued} \\ \text{in } \eta_{ab} \end{array} \right\rangle \quad \text{and}$$

$$\left\langle \psi(\eta_2)\sigma(\eta_3)\sigma(\eta_4) \prod_{i=1}^N \psi(z_i) \right\rangle = \frac{\eta_{34}^{3/8}}{\eta_{23}^{1/2} \eta_{24}^{1/2}} \left\langle \begin{array}{c} \text{single-valued} \\ \text{in } \eta_{ab} \end{array} \right\rangle.$$

Thus we finally obtain, for even number N of electrons,

$$\begin{aligned}\Psi_0 &= (\eta_{23}\eta_{24})^{\frac{1}{4}} \left\langle \begin{array}{c} \text{single-valued} \\ \text{in } \eta_{ab} \end{array} \right\rangle \\ \Psi_1 &= \frac{\sqrt{\eta_{12}\eta_{34}}}{(\eta_{23}\eta_{24})^{\frac{1}{4}}} \left\langle \begin{array}{c} \text{single-valued} \\ \text{in } \eta_{ab} \end{array} \right\rangle.\end{aligned}\quad (29)$$

We point out that the factors containing η_{ab} , hence the monodromies of the wave functions (29), are independent of whether the absolute value of \tilde{x} is bigger or smaller than 1 because considering $\eta_{12} \rightarrow 0$ actually means $|\tilde{x}| < 1$.

Now the read-out procedure, Eq. (17), which after the fusion $\eta_1 \rightarrow \eta_2$ is reduced to $\eta_{23} \rightarrow e^{2\pi i} \eta_{23}$, simply gives for the channel passing through P and Q in Fig. 1

$$\Psi_0 \rightarrow e^{i\frac{\pi}{2}} \Psi_0, \quad \text{while} \quad \Psi_1 \rightarrow e^{-i\frac{\pi}{2}} \Psi_1$$

so that the diagonal conductance is in agreement with Eqs. (5) and (6)

$$\sigma_{xx} \propto |t_{MN} + it_{PQ}|^2 \text{ for } \Psi_0, \quad \text{while} \quad \sigma_{xx} \propto |t_{MN} - it_{PQ}|^2 \text{ for } \Psi_1. \quad (30)$$

5 The NOT gate of Das Sarma et al.

The original idea of Ref. [28,29] behind the construction of the logical NOT gate in the setup shown on Fig. 1, is that when the quasiholes with coordinates η_1 and η_2 , localized on antidots 1 and 2, form the qubit [42] another quasihole with coordinate η_3 could tunnel between the front gates A and B (through an additional antidot located between A and B in order to guarantee a single quasi-hole tunneling) in such a way to flip the state of the qubit. The point is that this third quasi-hole actually encircles the quasi-hole localized on antidot 1 but not the second quasi-hole localized on antidot 2. More generally, while the read-out of the qubit is performed by taking η_3 around η_1 and η_2 , the NOT gate could be executed by taking η_3 around η_1 or η_2 but not both of them.

To understand this in more detail let us consider the simplest situation when the quasiholes are ordered $|\eta_1| > |\eta_2| > |\eta_3| > |\eta_4|$ and the quasi-hole at η_3 traverses a closed loop around the quasi-hole at η_2 , i.e.,

$$\text{NOT :} \quad \eta_{23} \rightarrow \lim_{t \rightarrow 1-} e^{2\pi i t} \eta_{23}, \quad \text{where} \quad t \in [0, 1) \quad (31)$$

with all other quasiholes coordinates remaining unchanged. Provided that the three quasiholes at η_1 , η_2 and η_3 are kept well-separated, after the tunneling of the third quasi-hole the 4-qh wave functions (14) are adiabatically transformed into new wave

functions which we shall find now. First the transformation (31) transforms the crossratio (15) according to $x \rightarrow e^{2\pi i}x$. Next we note that the Pfaffian wave functions $\Psi_{(ab)(cd)}$ are single-valued, so that they remain unchanged under the NOT transformation (31). Finally, the square root of x changes sign under the NOT transformation (31), i.e.,

$$\sqrt{x} \rightarrow \sqrt{e^{2\pi i}x} = e^{i\pi} \sqrt{x}.$$

The transformation of $\sqrt{1 \pm \sqrt{x}}$ is more subtle and depends on the absolute value of the crossratio x . When $|x| < 1$ we have $\sqrt{1 \pm \sqrt{x}} \rightarrow \sqrt{1 \mp \sqrt{x}}$ under the transformation (31), while if $|x| > 1$ $\sqrt{1 \pm \sqrt{x}} \rightarrow \pm \sqrt{1 \mp \sqrt{x}}$, because the transformation contour now encircles both branching points. Thus we find that the two 4-qh wave functions (14) transform under the NOT transformation (31) as follows

$$U_{\text{NOT}}^{\text{Das Sarma}} \begin{pmatrix} \Psi_{4\text{qh}}^{(0)} \\ \Psi_{4\text{qh}}^{(1)} \end{pmatrix} = \begin{pmatrix} 0 & 1 \\ 1 & 0 \end{pmatrix} \begin{pmatrix} \Psi_{4\text{qh}}^{(0)} \\ \Psi_{4\text{qh}}^{(1)} \end{pmatrix} \quad \text{for } |x| < 1, \quad \text{while} \quad (32)$$

$$U_{\text{NOT}}^{\text{Das Sarma}} \begin{pmatrix} \Psi_{4\text{qh}}^{(0)} \\ \Psi_{4\text{qh}}^{(1)} \end{pmatrix} = \begin{pmatrix} 0 & 1 \\ -1 & 0 \end{pmatrix} \begin{pmatrix} \Psi_{4\text{qh}}^{(0)} \\ \Psi_{4\text{qh}}^{(1)} \end{pmatrix} \quad \text{for } |x| > 1. \quad (33)$$

Thus we conclude that the transformation (31) indeed maps $\Psi_{4\text{qh}}^{(0)} \leftrightarrow \Psi_{4\text{qh}}^{(1)}$.

6 Exchange matrices and monodromy group representation of the Ising 4-point functions

The four-point correlation functions of the chiral spin field (12) in the Ising model can be shown to be [45]

$$F(\eta_1, \eta_2, \eta_3, \eta_4) \equiv \langle \sigma(\eta_1) \sigma(\eta_2) \sigma(\eta_3) \sigma(\eta_4) \rangle = F_+ + F_-, \quad \text{where} \\ F_{\pm}(\eta_1, \eta_2, \eta_3, \eta_4) = \frac{1}{\sqrt{2}} \left(\frac{\eta_{13}\eta_{24}}{\eta_{12}\eta_{14}\eta_{23}\eta_{34}} \right)^{\frac{1}{8}} \sqrt{1 \pm \sqrt{\frac{\eta_{14}\eta_{23}}{\eta_{13}\eta_{24}}}} \quad (34)$$

are the chiral conformal blocks, which could be expressed in terms of the fields σ_{\pm} with definite fermion parity as $F_{\pm} = \langle \sigma_+(\eta_1) \sigma_{\pm}(\eta_2) \sigma_+(\eta_3) \sigma_{\pm}(\eta_4) \rangle$.

The counter-clockwise exchange of the quasiparticles with coordinates η_1 and η_2 can be preformed by analytic continuation along the contour defined by

$$\eta'_1 = \frac{\eta_1 + \eta_2}{2} + e^{i\pi t} \frac{\eta_1 - \eta_2}{2}, \quad \eta'_2 = \frac{\eta_1 + \eta_2}{2} - e^{i\pi t} \frac{\eta_1 - \eta_2}{2}, \quad 0 \leq t \leq 1, \quad (35)$$

as shown in Fig. 6. Executing this transformation and taking the limit $t \rightarrow 1_-$ we

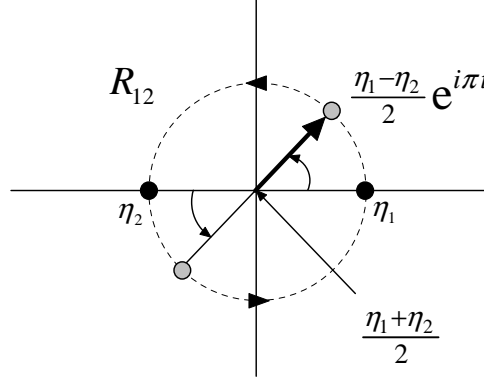


Fig. 6. Counter-clockwise exchange R_{12} of coordinates η_1 and η_2 performed by taking the limit $t = 0 \rightarrow 1_-$ in Eq. (35).

obtain for the 4-pt functions (note that $\eta'_{12} = e^{i\pi} \eta_{12}$)

$$R_{12} F_K = \left(\frac{e^{-i\pi} \eta_{13} \eta_{24}}{\eta_{12} \eta_{14} \eta_{23} \eta_{34}} \right)^{\frac{1}{8}} \left(\frac{\eta_{14} \eta_{23}}{\eta_{13} \eta_{24}} \right)^{\frac{1}{4}} \sqrt{1 + \kappa \sqrt{\frac{\eta_{13} \eta_{24}}{\eta_{14} \eta_{23}}}} = e^{-i\frac{\pi}{8}} \sqrt{\kappa} F_K(\eta_a).$$

Therefore (fixing the signs of the square roots by the requirement that the R -matrices must satisfy the Yang–Baxter equations (37)) we get a diagonal matrix

$$R_{12} \begin{pmatrix} F_+ \\ F_- \end{pmatrix} = e^{-i\frac{\pi}{8}} \begin{pmatrix} 1 & 0 \\ 0 & i \end{pmatrix} \begin{pmatrix} F_+ \\ F_- \end{pmatrix}.$$

Precisely in the same way we can compute the exchange matrix R_{34} which takes precisely the same form in this basis. In order to compute the exchange matrix R_{23} we apply the coordinate transformation (35), after renaming $(\eta_1, \eta_2) \rightarrow (\eta_2, \eta_3)$, and use the identity

$$\sqrt{1 + \sqrt{x}} + i\lambda \sqrt{1 - \sqrt{x}} = \sqrt{2\lambda} i \sqrt{\sqrt{1-x} - i\lambda \sqrt{x}}$$

for $\lambda = \pm 1$. We obtain

$$R_{23} F_{\pm} = \frac{e^{-i\frac{\pi}{8}}}{\sqrt{2}} \left(\frac{\eta_{13} \eta_{24}}{\eta_{12} \eta_{14} \eta_{23} \eta_{34}} \right)^{\frac{1}{8}} \sqrt{\sqrt{1-x} \pm i\sqrt{x}} = \frac{e^{-i\frac{\pi}{8}}}{\sqrt{2}} e^{\pm i\frac{\pi}{4}} (F_+ \mp iF_-).$$

Thus, we can summarize our results for the elementary exchange matrices $R_{a,a+1}$

in the basis $\{F_+, F_-\}$

$$R_{12} = R_{34} = e^{-i\frac{\pi}{8}} \begin{pmatrix} 1 & 0 \\ 0 & i \end{pmatrix}, \quad R_{23} = \frac{e^{i\frac{\pi}{8}}}{\sqrt{2}} \begin{pmatrix} 1 & -i \\ -i & 1 \end{pmatrix}. \quad (36)$$

All other exchanges can be obtained from the elementary ones, e.g.,

$$R_{13} = R_{12}^{-1} R_{23} R_{12} = \frac{e^{i\frac{\pi}{8}}}{\sqrt{2}} \begin{pmatrix} 1 & 1 \\ -1 & 1 \end{pmatrix}, \quad \text{etc.}$$

6.1 Exchange matrices for the 4-quasiholes wave functions $\Psi_{4\text{qh}}^{(0,1)}$

The 4-quasiholes wave functions (14) are built up from the 4-point functions of the Ising model and the functions $\Psi_{(ab)(cd)}$ which are single-valued in the positions of the quasiholes. Now a natural question arises: is the braid-group representation for the 4-point functions (19) extended to a braid-group representation over the 4-quasihole functions? The answer is yes. The point is that when a quasihole traverses a closed loop, the 4-quasihole functions should acquire an additional phase proportional to the number of electrons inside the loop (or, to the area of the loop). This might lead to a projective representation of the braid group as looks to be the case in the the p -wave composite-fermion superconductor approach, where the quasihole is identified with a half-quantum vortex [9]. However, as can be seen in our approach directly from the 4-quasihole functions (14), each electron inside the loop contributes 2π to this phase because the quasiholes are by definition local with the electrons³. Thus the phase is insensitive to the number of electrons inside the loop, it only counts the number of quasiholes. Nevertheless it turns out that braid-group (or mapping class group) [2] representations in terms of CFT correlation functions are generically projective. The point is that the coordinates of the many-body wave functions, which in the CFT approach [33] are chiral correlation functions defined on the unit circle, could be naturally extended by analytic continuation to the vicinity of the unit disk. Then by CFT transformation these functions could be extended to the entire *compactified* complex plane, which is isomorphic to the two-dimensional sphere. Now, besides the Artin relations [2]

$$\begin{aligned} B_i B_j &= B_j B_i, & \text{for } |i - j| \geq 2 \\ B_i B_{i+1} B_i &= B_{i+1} B_i B_{i+1}, & \text{where } B_i = R_{i,i+1} \in \mathcal{B}_n, \end{aligned} \quad (37)$$

³ what could really change the phase is not the entire electron but the neutral Majorana fermion, which is non-local with the quasihole

for the generators B_i ($i = 1, \dots, n-1$) of \mathcal{B}_n , the representation of the braid group on the sphere should satisfy one more relation [2]

$$B_1 B_2 \cdots B_{n-2} B_{n-1}^2 B_{n-2} \cdots B_2 B_1 = \mathbb{I}.$$

As can be seen by direct computation the above relation is satisfied by the elementary exchange matrices of the chiral CFT correlators only up to phase so that the braid-group representation is projective.

In the rest of this subsection we will show that from the exchange matrices for the functions F_{\pm} we could obtain the corresponding matrices in the basis $\{\Psi_{4\text{qh}}^{(0)}, \Psi_{4\text{qh}}^{(1)}\}$ in the form [46]

$$R_{12}^{(4)} = R_{34}^{(4)} = \begin{pmatrix} 1 & 0 \\ 0 & i \end{pmatrix}, \quad R_{23}^{(4)} = \frac{e^{i\frac{\pi}{4}}}{\sqrt{2}} \begin{pmatrix} 1 & -i \\ -i & 1 \end{pmatrix}, \quad (38)$$

where the superscript “(4)” is to remind us that these matrices are computed in the basis of the 4-quasihole states (14). Consider, for instance, the transformation (35) acting on the 4-quasihole wave functions (14). It changes $x \rightarrow 1/x$ and $\Psi_{(13)(24)} \leftrightarrow \Psi_{(14)(23)}$ so that

$$R_{12}^{(4)} \Psi_{4\text{qh}}^{(0,1)} = \frac{(\eta_{23}\eta_{14})^{\frac{1}{4}}}{\sqrt{1 \pm \sqrt{\frac{1}{x}}}} \left(\Psi_{(14)(23)} \pm \frac{1}{\sqrt{x}} \Psi_{(13)(24)} \right).$$

Expressing $\eta_{23}\eta_{14} = \eta_{13}\eta_{24}x$ and taking out $\sqrt{\pm\sqrt{1/x}}$ from the denominator we obtain the exchange matrix $R_{12}^{(4)}$ in the basis (14) as in Eq. (38). Notice that there is no more $e^{-i\pi/8}$ in this matrix. At this point the Yang–Baxter equations (37) imply that if there is a braid-group representation over the 4-quasihole wave functions (14) they must be obtained from Eq. (36) by multiplying all exchange matrices with $e^{i\pi/8}$. Because $R_{12}^{(4)}$ is diagonal it could be directly obtained by first fusing $\eta_1 \rightarrow \eta_2$ and then interpreting the exchange as $\eta_{12} \rightarrow e^{i\pi}\eta_{12}$, which gives the same result. Indeed, it follows from Eq. (29) that when $\eta'_1 = \eta_2 - e^{i\pi}\eta_{12}$, $\eta'_2 = \eta_2$, which is equivalent to $R_{12}^{(4)}$ the two functions Ψ_0 and Ψ_1 in Eq. (29) are multiplied by 1 and i respectively (note that the expression in the $\langle \dots \rangle$ in Eq. (29) is actually independent of η_1).

Next, instead of computing $R_{23}^{(4)}$ directly it is more convenient to compute $R_{13}^{(4)}$, following Ref. [39], and then use the identity

$$R_{23}^{(4)} = R_{12}^{(4)} R_{13}^{(4)} \left(R_{12}^{(4)} \right)^{-1}. \quad (39)$$

To this end we first apply the coordinate transformation

$$\eta'_1 = \eta_3, \quad \eta'_2 = \eta_2, \quad \eta'_3 = \eta_1, \quad \eta'_4 = \eta_4, \quad \text{such that} \quad \eta'_{13} = e^{i\pi} \eta_{13},$$

$x \rightarrow \tilde{x} = 1 - x$ and $\Psi_{(13)(24)} \rightarrow \Psi_{(13)(24)}$, while $\Psi_{(14)(23)} \rightarrow \Psi_{(12)(34)}$. Then, using the Nayak–Wilczek identity [39] (note the misprints in Eq. (3.8) there)

$$(1-x)\Psi_{(12)(34)} = \Psi_{(13)(24)} - x\Psi_{(14)(23)}, \quad \text{as well as}$$

$$\sqrt{1 + \sqrt{1 - \tilde{x}}} \pm \sqrt{1 - \sqrt{1 - \tilde{x}}} = \pm \sqrt{2} \sqrt{1 \pm \sqrt{\tilde{x}}}, \quad (40)$$

it is not difficult to derive $R_{13}^{(4)}$, hence obtain $R_{23}^{(4)}$ by Eq. (39), i.e.,

$$R_{13}^{(4)} \begin{pmatrix} \Psi_{4\text{qh}}^{(0)} \\ \Psi_{4\text{qh}}^{(1)} \end{pmatrix} = \frac{e^{i\frac{\pi}{4}}}{\sqrt{2}} \begin{pmatrix} 1 & 1 \\ -1 & 1 \end{pmatrix} \begin{pmatrix} \Psi_{4\text{qh}}^{(0)} \\ \Psi_{4\text{qh}}^{(1)} \end{pmatrix}.$$

The sign ambiguity in front of the square root in the right-hand side of Eq. (40) comes from taking a square root and is not directly linked to the sign under the square root on the right. In order to fix this sign we use Eq. (39) and the fact that the NOT gate $U_{\text{NOT}}^{\text{Das Sarma}}$ for $|x| < 1$, that we obtained in Eq. (32) directly in terms of the 4-quasiholes wave functions monodromies in Sect. 5, is actually the square of the exchange matrix $R_{23}^{(4)}$, i.e.,

$$\left(R_{23}^{(4)} \right)^2 \Psi_{4\text{qh}}^{(0,1)} = \Psi_{4\text{qh}}^{(1,0)} \quad \Rightarrow \quad \left(R_{23}^{(4)} \right)^2 = \begin{pmatrix} 0 & 1 \\ 1 & 0 \end{pmatrix}.$$

Remark 1 *The relevance of the Pfaffian qubit for quantum computation can be emphasized once again. Because the monodromy matrix $\left(R_{23}^{(4)} \right)^2$ coincides with the NOT gate in the 4-quasiholes states basis, the matrix $R_{23}^{(4)}$ should be identified with $\sqrt{\text{NOT}}$, which cannot be implemented in classical information theory [47]. As we shall see later this operation is crucial for the construction of the Hadamard gate, which is one of the most important single-qubit quantum gate.*

The monodromy transformations, corresponding to the elementary exchanges, i.e., the squares of $R_{a,a+1}^{(4)}$ representing a complete counter-clockwise cycle of the particle with label $a+1$ around that with label a ,

$$\left(R_{12}^{(4)} \right)^2 = \left(R_{34}^{(4)} \right)^2 = \begin{pmatrix} 1 & 0 \\ 0 & -1 \end{pmatrix}, \quad \left(R_{23}^{(4)} \right)^2 = \begin{pmatrix} 0 & 1 \\ 1 & 0 \end{pmatrix},$$

form a subgroup of the braid group called the monodromy group. The monodromy group representation is thus generated by the Pauli matrices σ_1 and σ_3 , or, al-

ternatively, by the two elements⁴ $S = i\sigma_2$, $R = \sigma_1$, such that $S^4 = R^2 = \mathbb{I}$ and $R^{-1}SR = S^{-1}$. Therefore the image of the monodromy group is isomorphic to the finite non-Abelian group \mathcal{D}_4 [48,49], known as the symmetry group of the square, which has 8 elements typically given in the two-dimensional representation as

$$\mathcal{D}_4 \equiv \{\pm\mathbb{I}_2, \pm\sigma_1, \pm i\sigma_2, \pm\sigma_3\},$$

where σ_i are the three Pauli matrices. The monodromy group \mathcal{M}_n is in general a normal subgroup of the braid group \mathcal{B}_n and the factor-group

$$\mathcal{B}_n/\mathcal{M}_n \simeq \mathcal{S}_n$$

is isomorphic to the permutation group \mathcal{S}_n . Therefore, the fact that the monodromy group representation $\mathcal{M}_4 = \mathcal{D}_4$ for the 4-pt functions is finite implies that the braid group representation in this case is a finite group whose order could be shown to be $|\text{Image}(\mathcal{B}_4)| = 96$. The order of the representation of the braid group \mathcal{B}_6 is $|\text{Image}(\mathcal{B}_6)| = 46080 = 2^6 6!$, while that of the monodromy subgroup is $|\text{Image}(\mathcal{M}_6)| = 32$. Similarly, the order of the representation of the braid group \mathcal{B}_8 is $|\text{Image}(\mathcal{B}_8)| = 5160960 = 2^7 8!$, and that of its monodromy subgroup is $|\text{Image}(\mathcal{M}_8)| = 128$. These numbers have been obtained by direct enumeration of the distinct matrices, produced by multiplying the elementary braid matrices, in the corresponding braid-group representation using the Dimino's algorithm [50]. In general the image of the representation of the braid group \mathcal{B}_{2n} , for $n \geq 3$, over the $2n$ -point functions of the Ising model is [51]

$$|\text{Image}(\mathcal{B}_{2n})| = \begin{cases} 2^{2n-1}(2n)! & \text{for } n = \text{even} \\ 2^{2n}(2n)! & \text{for } n = \text{odd} \end{cases}.$$

While this may look very nice as a mathematical fact it is fairly disappointing from the perspective of topological quantum computation. The point is that our intention in TQC is to implement quantum gates by simply exchanging quasiparticles positions and the finite braid-group representation implies that we could generate only finite number of gates with the Pfaffian qubit. Therefore it cannot be used for universal TQC where we would like to efficiently implement any unitary matrix (with a given precision). However, the set of quantum gates that could be realized by braiding of Pfaffian quasiparticles is known to be a Clifford group, which plays a central role in quantum error correction codes, so their topologically protected construction is fairly important. Moreover, in the next Section we will try to circumvent this restriction by finding a unitary transformation, which does not belong

⁴ note that the second Pauli matrix here appears in this context naturally multiplied by i and this is in accord with the standard quantum computation conventions [24]

to the braid group, that could be used to construct a universal set of gates, and is topologically protected.

6.2 The read-out of the single-qubit state in terms of the exchange matrices

Instead of interpreting the read-out as “taking η_3 around η_4 ”, as we did in Sects. 3.1 and 3.2, we could use the exchange matrices (38) to directly “take η_3 around η_1 and η_2 ”. Again the measurement result depends on whether the absolute value of the crossratio (18) is smaller or bigger than 1. In the case $|\tilde{x}| < 1$, which is the usual situation when, e.g., $|\eta_1| > |\eta_2| > |\eta_3| > |\eta_4|$, as shown on Fig. 7, the operator corresponding to the transportation of η_3 around η_1 and η_2 is

$$U_{\text{read-out}}^{(|\tilde{x}| < 1)} = R_{23}R_{12}^2R_{23} = \frac{e^{i\frac{\pi}{2}}}{2} \begin{pmatrix} 1 & -i \\ -i & 1 \end{pmatrix} \begin{pmatrix} 1 & 0 \\ 0 & -1 \end{pmatrix} \begin{pmatrix} 1 & -i \\ -i & 1 \end{pmatrix} = \begin{pmatrix} i & 0 \\ 0 & -i \end{pmatrix},$$

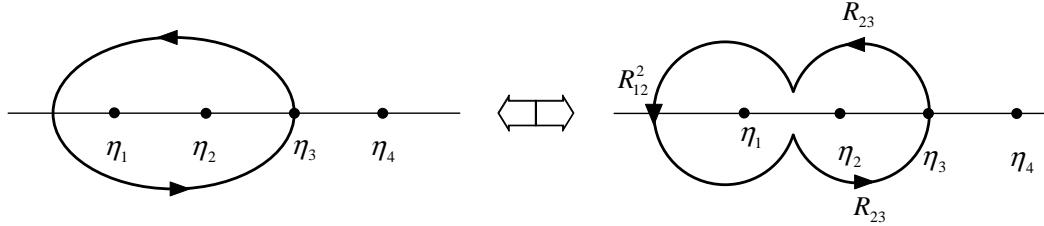


Fig. 7. The read-out for $|\tilde{x}| < 1$ in terms of the elementary exchange matrices.

and the result is the same as Eq. (21). If on the other hand $|\tilde{x}| > 1$, which can be considered as, e.g., $|\eta_2| < |\eta_3|$, because using the the CFT symmetry we can express $\tilde{x} = \eta_3/\eta_2$. In this case the read-out operation corresponds to Fig. 8, is

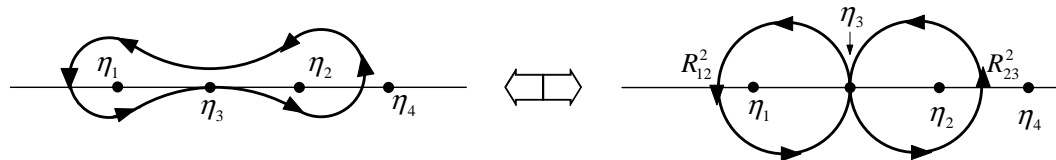


Fig. 8. The read-out for $|\tilde{x}| > 1$ in terms of the elementary exchange matrices.

$$U_{\text{read-out}}^{(|\tilde{x}| > 1)} = R_{12}^2R_{23}^2 = \begin{pmatrix} 1 & 0 \\ 0 & -1 \end{pmatrix} \begin{pmatrix} 0 & 1 \\ 1 & 0 \end{pmatrix} = \begin{pmatrix} 0 & 1 \\ -1 & 0 \end{pmatrix}$$

and this is (up to phase) identical with Eq. (24).

7 Single-qubit gates constructed from elementary exchange matrices

In this Section we shall implement by quasi-hole braiding the following single-qubit gates: the Hadamard gate H , Pauli gates X , Y , Z , and the phase gate S [24]). In Sect. 8.4 we shall also construct entirely in terms of quasi-hole braidings the Controlled-NOT gate. While not sufficient for universal QC, these gates are known to form a Clifford group [38] and could in principle be used for universal quantum computation provided that we can create the so-called *magic states* [38]. The only single-qubit gate that we cannot construct directly by braiding is the $\pi/8$ gate T [24]). However, instead of the $\pi/8$ gate one we could use the three-qubit Toffoli gate [24]).

The Hadamard gate H is of central importance for any QC scheme. It is worth stressing that the Hadamard gate is the only gate which must be added to a universal classical computer (based on the Toffoli gate) in order to make it a universal quantum computer [52]. In the TQC with Pfaffian qubits it can be used to create special superpositions, called the Bell states (or EPR states) [24], that can be constructed in no other way. In addition H is one of the building blocks of the quantum Fourier transform [24]). The Hadamard gate in the Pfaffian TQC scheme can be expressed in terms of three elementary braidings of the 4-quasihole states (14), namely ⁵,

$$H \simeq R_{13}R_{12}^2 = R_{12}^{-1}R_{23}R_{12}^{-1} = \frac{e^{i\frac{\pi}{4}}}{\sqrt{2}} \begin{pmatrix} 1 & 1 \\ 1 & -1 \end{pmatrix}. \quad (41)$$

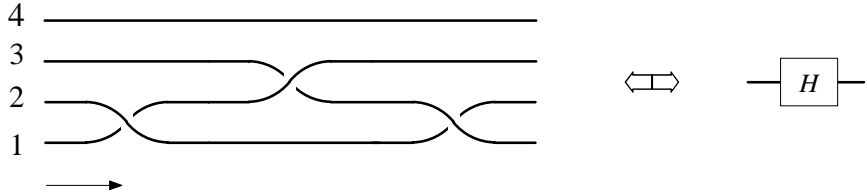


Fig. 9. Braiding diagram for the Hadamard gate (41) and its symbol (on the right) in standard quantum-computation notation

It would be convenient to represent these braidings in braid diagrams, such as Fig. (9). The first and the third braids in Fig. (9) are in clockwise direction and correspond to the inverse exchanges R_{12}^{-1} , while the second exchange is in counter-clockwise direction and corresponds to R_{23} .

⁵ the results in this Section have been originally announced in Ref. [46]; here we give a detailed derivation

The Pauli X gate, known also as the NOT gate, which was first implemented for the Pfaffian qubit in Ref. [28], could be executed by two elementary exchanges as

$$X \equiv R_{23}^2 = \begin{pmatrix} 0 & 1 \\ 1 & 0 \end{pmatrix}$$

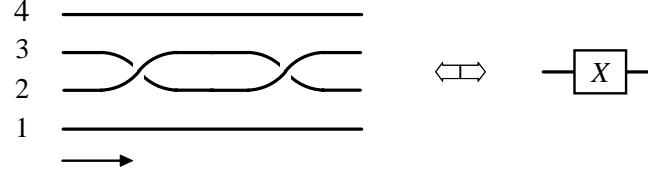


Fig. 10. Braiding diagram for the Pauli X gate and its quantum-computation symbol

and the corresponding braid diagram is shown on Fig. 10. Similarly, the Y gate, which is usually defined in quantum computation literature without the imaginary unit, is realized by 4 elementary exchanges as follows

$$Y \equiv R_{12}^{-1} R_{23}^2 R_{12} = \begin{pmatrix} 0 & 1 \\ -1 & 0 \end{pmatrix}$$

and the corresponding braid diagram is shown on Fig. 11. The Pauli Z gate [24] can

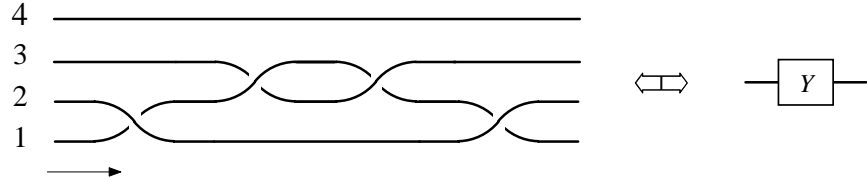


Fig. 11. Braiding diagram for the Pauli Y gate

be realized in two different ways by two elementary exchanges as

$$Z \equiv R_{12}^2 = R_{34}^2 = \begin{pmatrix} 1 & 0 \\ 0 & -1 \end{pmatrix}$$

and the braid diagram for the first of them is shown on Fig. 12. Finally, the phase gate S , which can also be realized in two different ways by a single elementary exchange,

$$S \equiv R_{12} = R_{34} = \begin{pmatrix} 1 & 0 \\ 0 & i \end{pmatrix}$$

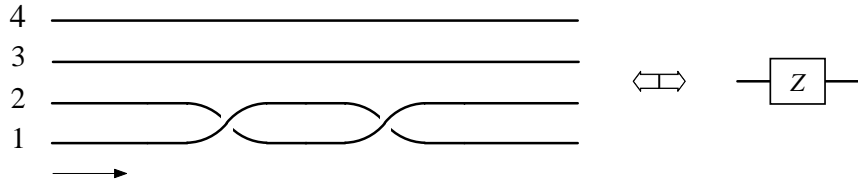


Fig. 12. Braiding diagram for the Pauli Z gate

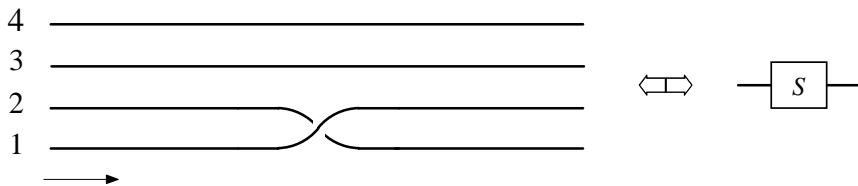


Fig. 13. Braiding diagram for the phase gate S

and the first of them, $S = R_{12}$, is shown graphically on Fig. 13. Notice that $S^2 = Z$ as it should be.

The only single-qubit gate which cannot be implemented directly in terms of quasi-holes braiding is the $\pi/8$ -gate $T = \text{diag} \left(1, e^{i\pi/4} \right)$ [24] because $\det T = e^{i\pi/4}$, while $\det \left(R_{a,a+1}^{(4)} \right) = i$ for all a . Instead of T we shall propose to construct the Toffoli gate.

8 Two-qubits construction and two-qubit gates

In order to realize two qubits, which belong to \mathbb{C}^2 , we need at least 4-dimensional space. Recalling that the dimension of the excited Pfaffian states with $2n$ quasiholes at fixed positions [39] is $\dim \mathcal{H}_{2n} = 2^{n-1}$ we consider the 6-quasihole states. Before we explain how to construct the two-qubit states let us recall that the single qubit states can be written as

$$|0\rangle \equiv \langle \sigma_+ \sigma_+ \sigma_+ \sigma_+ \rangle, \quad |1\rangle \equiv \langle \sigma_+ \sigma_- \sigma_+ \sigma_- \rangle,$$

where we take the convention that the first two σ fields determine the state of the qubit while the last two guarantee the preservation of the fermion parity, so that basically $|0\rangle \simeq \sigma_+ \sigma_+$, while $|1\rangle \simeq \sigma_+ \sigma_-$, which is agreement with our definition

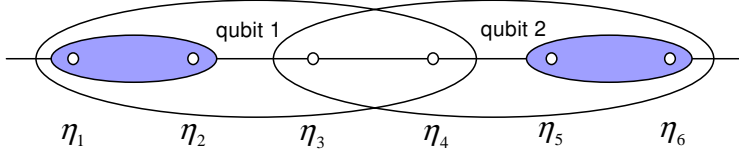


Fig. 14. Two qubits, realized by quasiholes with coordinates $(\eta_1, \eta_2, \eta_3, \eta_4)$ and $(\eta_3, \eta_4, \eta_5, \eta_6)$, spanning the needed 4 dimensional space \mathbb{C}^2 . The state of qubit 1 is determined by the quasiholes with positions (η_1, η_2) , while the state of qubit 2 by the quasiholes with positions (η_5, η_6) and that is why these two groups were shaded. The state of the quasiholes with coordinates (η_3, η_4) depends on both quasihole pairs (η_1, η_2) and (η_5, η_6) .

of the qubit because of the fusion rules $\sigma_+ \sigma_+ \sim \mathbb{I}$ and $\sigma_+ \sigma_- \sim \psi$.

The two-qubit basis is defined here by the convention that the first two quasiholes form the first qubit while the last two quasiholes form the second qubit

$$\begin{aligned} |00\rangle &\equiv \langle \sigma_+ \sigma_+ \sigma_+ \sigma_+ \sigma_+ \sigma_+ \rangle, & |01\rangle &\equiv \langle \sigma_+ \sigma_+ \sigma_+ \sigma_- \sigma_+ \sigma_- \rangle \\ |10\rangle &\equiv \langle \sigma_+ \sigma_- \sigma_+ \sigma_- \sigma_+ \sigma_+ \rangle, & |11\rangle &\equiv \langle \sigma_+ \sigma_- \sigma_+ \sigma_+ \sigma_+ \sigma_- \rangle. \end{aligned} \quad (42)$$

This is convenient since if we fuse the first two quasiholes this would project to the second qubit, while if we fuse the last two quasiholes this would project to the first qubit, i.e.,

$$|\alpha\beta\rangle_{\eta_1 \rightarrow \eta_2} |\beta\rangle, \quad |\alpha\beta\rangle_{\eta_5 \rightarrow \eta_6} |\alpha\rangle. \quad (43)$$

Then the third and the fourth quasiholes are fixed by the conservation of the fermion parity, i.e., if e_i is the parity of σ_{e_i} , consider the correlation function with γ_F plugged in the middle. This gives

$$\langle \sigma_{e_1} \sigma_{e_2} \sigma_{e_3} \gamma_F \sigma_{e_4} \sigma_{e_5} \sigma_{e_6} \rangle = e_1 e_2 e_3 \langle \sigma_{e_1} \sigma_{e_2} \sigma_{e_3} \sigma_{e_4} \sigma_{e_5} \sigma_{e_6} \rangle$$

if we move γ_F to the left or $e_4 e_5 e_6 \langle \sigma_{e_1} \sigma_{e_2} \sigma_{e_3} \sigma_{e_4} \sigma_{e_5} \sigma_{e_6} \rangle$ if we move it to the right. Therefore we obtain the fermion parity rule

$$e_1 e_2 e_3 = e_4 e_5 e_6 \quad \Rightarrow \quad e_3 e_4 = e_1 e_2 e_5 e_6,$$

where the last equality follows from $e_i^2 = 1$. Thus we have only 4 independent states in the space of 6-quasiholes with fixed positions, which correspond to Eq. (42).

8.1 Exchange matrices for 6-quasiholes

The braid group representation over the 6-pt functions is generated by the elementary exchanges $R_{12}^{(6)}, R_{23}^{(6)}, R_{34}^{(6)}, R_{45}^{(6)}$ and $R_{56}^{(6)}$. We shall construct them explicitly by using the operator-product expansions of the Ising model and the projections to the single-qubit states along the lines of Ref. [46].

The construction (42) of the two-qubit states allows to derive the 6-quasiholes exchange matrices in terms of those for the 4 quasiholes. In order to obtain the exchange $R_{12}^{(6)}$ we may first fuse $\eta_5 \rightarrow \eta_6$, because the state of the first qubit is independent of η_5 and η_6 , and use the projections (43). In more detail, we have

$$\begin{aligned} |00\rangle_{\eta_5 \rightarrow \eta_6} &\rightarrow \langle \sigma_+ \sigma_+ \sigma_+ \sigma_+ \rangle, & |01\rangle_{\eta_5 \rightarrow \eta_6} &\rightarrow \langle \sigma_+ \sigma_+ \sigma_+ \sigma_- \psi \rangle \\ |10\rangle_{\eta_5 \rightarrow \eta_6} &\rightarrow \langle \sigma_+ \sigma_- \sigma_+ \sigma_- \rangle, & |11\rangle_{\eta_5 \rightarrow \eta_6} &\rightarrow \langle \sigma_+ \sigma_- \sigma_+ \sigma_+ \psi \rangle. \end{aligned} \quad (44)$$

Now the exchange $\eta_1 \leftrightarrow \eta_2$ is represented by the action of $R_{12}^{(4)}$, which we take from Eq. (38), i.e.,

$$\begin{aligned} |00\rangle_{\eta_1 \leftrightarrow \eta_2} &\rightarrow \langle \sigma_+ \sigma_+ \sigma_+ \sigma_+ \rangle, & |01\rangle_{\eta_1 \leftrightarrow \eta_2} &\rightarrow \langle \sigma_+ \sigma_+ \sigma_+ \sigma_- \psi \rangle \\ |10\rangle_{\eta_1 \leftrightarrow \eta_2} &\rightarrow i \langle \sigma_+ \sigma_- \sigma_+ \sigma_- \rangle, & |11\rangle_{\eta_1 \leftrightarrow \eta_2} &\rightarrow i \langle \sigma_+ \sigma_- \sigma_+ \sigma_+ \psi \rangle \end{aligned}$$

and restoring back the second qubit we obtain in the basis (42)

$$R_{12}^{(6)} = \begin{pmatrix} 1 & 0 & 0 & 0 \\ 0 & 1 & 0 & 0 \\ 0 & 0 & i & 0 \\ 0 & 0 & 0 & i \end{pmatrix} = R_{12}^{(4)} \otimes \mathbb{I}_2. \quad (45)$$

Now let us compute the exchange matrix $R_{23}^{(6)}$. Again we can fuse $\eta_5 \rightarrow \eta_6$ and use Eq. (44). The exchange $\eta_2 \leftrightarrow \eta_3$ is represented by the action of $R_{23}^{(4)}$, from Eq. (38), i.e.,

$$\begin{aligned} |00\rangle_{\eta_2 \leftrightarrow \eta_3} &\rightarrow \frac{e^{i\frac{\pi}{4}}}{\sqrt{2}} \langle \sigma_+ \sigma_+ \sigma_+ \sigma_+ \rangle - i \frac{e^{i\frac{\pi}{4}}}{\sqrt{2}} \langle \sigma_+ \sigma_- \sigma_+ \sigma_- \rangle, \\ |01\rangle_{\eta_2 \leftrightarrow \eta_3} &\rightarrow \frac{e^{i\frac{\pi}{4}}}{\sqrt{2}} \langle \sigma_+ \sigma_+ \sigma_+ \sigma_- \psi \rangle - i \frac{e^{i\frac{\pi}{4}}}{\sqrt{2}} \langle \sigma_+ \sigma_- \sigma_+ \sigma_+ \psi \rangle, \\ |10\rangle_{\eta_2 \leftrightarrow \eta_3} &\rightarrow \frac{e^{i\frac{\pi}{4}}}{\sqrt{2}} \langle \sigma_+ \sigma_- \sigma_+ \sigma_- \rangle - i \frac{e^{i\frac{\pi}{4}}}{\sqrt{2}} \langle \sigma_+ \sigma_+ \sigma_+ \sigma_+ \rangle, \end{aligned}$$

$$|11\rangle \underset{\eta_2 \leftrightarrow \eta_3}{\rightarrow} \frac{e^{i\frac{\pi}{4}}}{\sqrt{2}} \langle \sigma_+ \sigma_- \sigma_+ \sigma_+ \psi \rangle - i \frac{e^{i\frac{\pi}{4}}}{\sqrt{2}} \langle \sigma_+ \sigma_+ \sigma_+ \sigma_- \psi \rangle$$

and restoring back again the second qubit according to Eq. (44) we obtain in the basis (42)

$$R_{23}^{(6)} = \frac{e^{i\frac{\pi}{4}}}{\sqrt{2}} \begin{pmatrix} 1 & 0 & -i & 0 \\ 0 & 1 & 0 & -i \\ -i & 0 & 1 & 0 \\ 0 & -i & 0 & 1 \end{pmatrix} = R_{23}^{(4)} \otimes \mathbb{I}_2. \quad (46)$$

Precisely in the same way, by fusing first $\eta_1 \rightarrow \eta_2$, we can obtain the 6-quasiholes exchange matrices

$$R_{45}^{(6)} = \frac{e^{i\frac{\pi}{4}}}{\sqrt{2}} \begin{pmatrix} 1 & -i & 0 & 0 \\ -i & 1 & 0 & 0 \\ 0 & 0 & 1 & -i \\ 0 & 0 & -i & 1 \end{pmatrix} = \mathbb{I}_2 \otimes R_{23}^{(4)}, \quad \text{and} \quad (47)$$

$$R_{56}^{(6)} = \begin{pmatrix} 1 & 0 & 0 & 0 \\ 0 & i & 0 & 0 \\ 0 & 0 & 1 & 0 \\ 0 & 0 & 0 & i \end{pmatrix} = \mathbb{I}_2 \otimes R_{34}^{(4)}. \quad (48)$$

The exchange matrix $R_{34}^{(6)}$ cannot be obtained simply in this way because the quasiholes at η_3 and η_4 depend on the states of both qubits so that fusing either (η_1, η_2) or (η_5, η_6) would change the state of the quasi-hole pair at (η_3, η_4) . As we shall see in Sect. 8.2 this entanglement of the two qubits allows us to construct immediately the Controlled-Z gate. Notice, however, that $R_{34}^{(6)}$ must be diagonal and therefore could be directly determined by simply using the OPE for the fusion $\eta_3 \rightarrow \eta_4$ alone. One way to see this is that if $R_{34}^{(6)}$ were non-diagonal the exchange of quasiholes at η_3 and η_4 would create a coherent superposition of the states $\mathbb{I}|NS\rangle$ and $\psi|NS\rangle$ in the Neveu–Schwartz sector (states with even number of σ fields acting on the vacuum belong to the NS sector) which would be a violation of the superselection rule defined by the chiral fermion parity γ_F . In contrast, if there are odd number of σ ’s to the right of η_a and η_{a+1} acting on the vacuum then the fusion $\eta_a \rightarrow \eta_{a+1}$ generates $\mathbb{I}|R\rangle$ and $\psi|R\rangle$, which are in the Ramond sector where the chiral fermion parity is spontaneously broken [33], so that the above states could indeed form coherent superpositions. This explains why $R_{23}^{(6)}$ and $R_{45}^{(6)}$ could be non-diagonal, while $R_{12}^{(6)}$, $R_{34}^{(6)}$ and $R_{56}^{(6)}$ have to be diagonal. Thus, using the (neutral part of the) OPE (27), we have

$$|00\rangle \underset{\eta_3 \rightarrow \eta_4}{\rightarrow} \eta_{34}^{-1/8} \langle \sigma_+ \sigma_+ \sigma_+ \sigma_+ \rangle, \quad |01\rangle \underset{\eta_3 \rightarrow \eta_4}{\rightarrow} \eta_{34}^{3/8} \langle \sigma_+ \sigma_+ \psi \sigma_+ \sigma_- \rangle$$

$$|10\rangle_{\eta_3 \rightarrow \eta_4} \xrightarrow{\eta_{34}^{3/8}} \langle \sigma_+ \sigma_- \psi \sigma_+ \sigma_+ \rangle, \quad |11\rangle_{\eta_3 \rightarrow \eta_4} \xrightarrow{\eta_{34}^{-1/8}} \langle \sigma_+ \sigma_- \sigma_+ \sigma_- \rangle. \quad (49)$$

Therefore, the exchange $\eta_3 \leftrightarrow \eta_4$, which simply transforms $\eta_{34} \rightarrow e^{i\pi} \eta_{34}$, leads to

$$\begin{aligned} |00\rangle_{\eta_3 \leftrightarrow \eta_4} &\xrightarrow{e^{-i\frac{\pi}{8}} \eta_{34}^{-1/8}} \langle \sigma_+ \sigma_+ \sigma_+ \sigma_+ \rangle, \\ |01\rangle_{\eta_3 \leftrightarrow \eta_4} &\xrightarrow{i e^{-i\frac{\pi}{8}} \eta_{34}^{3/8}} \langle \sigma_+ \sigma_+ \psi \sigma_+ \sigma_- \rangle \\ |10\rangle_{\eta_3 \leftrightarrow \eta_4} &\xrightarrow{i e^{-i\frac{\pi}{8}} \eta_{34}^{3/8}} \langle \sigma_+ \sigma_- \psi \sigma_+ \sigma_+ \rangle, \\ |11\rangle_{\eta_3 \leftrightarrow \eta_4} &\xrightarrow{e^{-i\frac{\pi}{8}} \eta_{34}^{-1/8}} \langle \sigma_+ \sigma_- \sigma_+ \sigma_- \rangle. \end{aligned}$$

Taking into account that there is another $\eta_{34}^{1/8}$, coming from the $u(1)$ component of the quasi-hole operator, we find the exchange matrix $R_{34}^{(6)}$ in the basis (42) to be

$$R_{34}^{(6)} = \begin{pmatrix} 1 & 0 & 0 & 0 \\ 0 & i & 0 & 0 \\ 0 & 0 & i & 0 \\ 0 & 0 & 0 & 1 \end{pmatrix}. \quad (50)$$

Unlike the other 6 quasiholes exchange matrices, $R_{34}^{(6)}$ is not a factorized tensor product of the 4 quasiholes exchange matrices. Instead, there is an additional built-in structure in this representation of the braid group, which will eventually allow us to construct the Controlled-Z gate.

It is easy to check that the 6-quasiholes exchange matrices (45), (46), (47), (48) and (50) indeed satisfy the Artin relations (37) for the braid group \mathcal{B}_6 [2], including the Yang–Baxter equations. As mentioned before, using the Dimino’s algorithm [50] we can explicitly obtain the entire group generated by the matrices (45), (46), (50), (47) and (48), giving the orders of the representation of the braid group \mathcal{B}_6 and its monodromy subgroup

$$|\text{Image}(\mathcal{B}_6)| = 46080, \quad |\text{Image}(\mathcal{M}_6)| = 32.$$

8.2 The Controlled-Z gate in terms of 6-quasiholes braidings

Using the explicit expressions for the 6-pt R -matrices, Eqs. (45), (50) and (48), it is straight forward to construct the most important two-qubit gates—the CNOT or

CZ gates in terms of the braid matrices, e.g.,

$$\text{CZ} = R_{12}^{(6)} (R_{34}^{(6)})^{-1} R_{56}^{(6)} = \begin{pmatrix} 1 & 0 & 0 & 0 \\ 0 & 1 & 0 & 0 \\ 0 & 0 & 1 & 0 \\ 0 & 0 & 0 & -1 \end{pmatrix}. \quad (51)$$

Some insight into the CZ construction may be gained from the identity [24]

$$\text{CZ} = e^{i\frac{\pi}{4}} e^{i\frac{\pi}{4}Z_1 Z_2} e^{-i\frac{\pi}{4}Z_1} e^{-i\frac{\pi}{4}Z_2},$$

where Z_1 and Z_2 are the Z gates acting on qubit 1 and 2 respectively. Because these matrices are diagonal and square to \mathbb{I} it is not difficult to prove that their exponents are actually equal (up to overall phases) to the matrices $R_{12}^{(6)}, R_{56}^{(6)}$ respectively, while the exponent of $Z_1 Z_2$ is proportional to the inverse of $R_{34}^{(6)}$.

The braid diagram for the 6-quasihole exchanges corresponding to Eq. (51) is shown on Fig. 15. In plotting Fig. 15 we have used that the three R -matrices en-

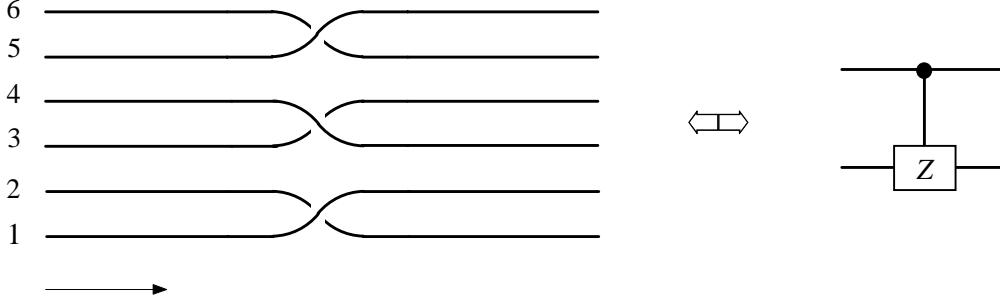


Fig. 15. The braid diagram for the Controlled-Z gate realized by 3 commuting elementary 6-quasiparticle braidings defined in Eq. (51). The symbol on the right is the standard quantum-computation notation for CZ.

tering Eq. (51) are diagonal and therefore commute, which also follows from the Artin relations (37), so that the order of the exchanges is not important. Note the remarkable simplicity of this realization of the CZ gate—just three elementary exchanges. This is one of the main advantages of the two-qubit construction in terms of 6 quasiholes presented in Sect. 8.

8.3 Single-qubit gates in the two-qubit basis

Before we continue, it is important to show that we can efficiently express the single-qubit gates into the two-qubit basis (42). The point is that the exchange matrices for 4 quasiholes, which represent the single-qubit operations, belong to the

braid group \mathcal{B}_4 while those for the two-qubit gates are expressed in terms of braid matrices from the braid group \mathcal{B}_6 and the former have different structure from the latter. Physically, the embedding of the one-qubit gates into the two-qubit system is non-trivial because the entanglement creates non-local effects between the two qubits. Nevertheless, the single-qubit construction in terms of 4 quasiholes exchanges is certainly instructive for the representation of these gates in the two-qubit basis. For our purposes it would be convenient to construct these gates explicitly.

The Hadamard gate acting on the first qubit can be expressed as

$$H_1 \simeq H \otimes \mathbb{I}_2 = \left(R_{12}^{(6)} \right)^{-1} \left(R_{23}^{(6)} \right)^{-1} \left(R_{12}^{(6)} \right)^{-1} = \frac{e^{-i\frac{\pi}{4}}}{\sqrt{2}} \begin{pmatrix} 1 & 0 & 1 & 0 \\ 0 & 1 & 0 & 1 \\ 1 & 0 & -1 & 0 \\ 0 & 1 & 0 & -1 \end{pmatrix},$$

while that acting on the second qubit should be identified with

$$H_2 \simeq \mathbb{I}_2 \otimes H = R_{56}^{(6)} R_{45}^{(6)} R_{56}^{(6)} = \frac{e^{i\frac{\pi}{4}}}{\sqrt{2}} \begin{pmatrix} 1 & 1 & 0 & 0 \\ 1 & -1 & 0 & 0 \\ 0 & 0 & 1 & 1 \\ 0 & 0 & 1 & -1 \end{pmatrix}. \quad (52)$$

Both Hadamard gates have similar structures to their single-qubit counterparts, yet, they are slightly different. This is surprising because adding an additional qubit is equivalent to introducing two more strands in the braid diagram and we expect that the two straight lines representing a trivial braiding in the new qubit should correspond to the the unit operator in a tensor product with the single-qubit gate acting on the old qubit. The point is that, however, the representation of the braid group \mathcal{B}_6 realized by the 6-quasihole Pfaffian wave functions naturally appear in a different basis, which is not a factorized tensor product of the representations of \mathcal{B}_4 over the 4-quasiholes Pfaffian wave functions. This is some kind of topological entanglement which seems to be common for all TQC schemes based on non-Abelian anyons realized in FQH systems.

The phase gates acting on the first and second qubits are respectively

$$S_1 = S \otimes \mathbb{I}_2 = R_{12}^{(6)} \quad \text{and} \quad S_2 = \mathbb{I}_2 \otimes S = R_{56}^{(6)}.$$

The embeddings of the other single-qubits into the two-qubit basis follow from these of H and S because $Z = S^2$ and $HZH = X$.

8.4 The Controlled-NOT gate

Now that we know how to construct the Controlled-Z gate, and how to embed the single-qubits gates, entirely in terms of 6-quasiholes braidings, the CNOT gate is readily computed with the help of the target-qubit Hadamard gate (52), i.e.,

$$\text{CNOT} = H_2 \text{ CZ } H_2 = R_{56} R_{45} R_{56}^{-1} R_{34}^{-1} R_{12} R_{45} R_{56} \simeq \begin{pmatrix} 1 & 0 & 0 & 0 \\ 0 & 1 & 0 & 0 \\ 0 & 0 & 0 & 1 \\ 0 & 0 & 1 & 0 \end{pmatrix}. \quad (53)$$

We used here that the target-qubit Hadamard gate could be executed by 3 exchanges, according to Eq. (52), as well as the property $(R_{56})^4 = \mathbb{I}_4$ and some of the Artin relations (37) for the 6-quasiholes exchange matrices. An equivalent realization of CNOT, which gives precisely the same result as in Eq. (53), could be given in terms of other 7 elementary exchanges

$$\text{CNOT} = R_{34}^{-1} R_{45} R_{34} R_{12} R_{56} R_{45} R_{34}^{-1}. \quad (54)$$

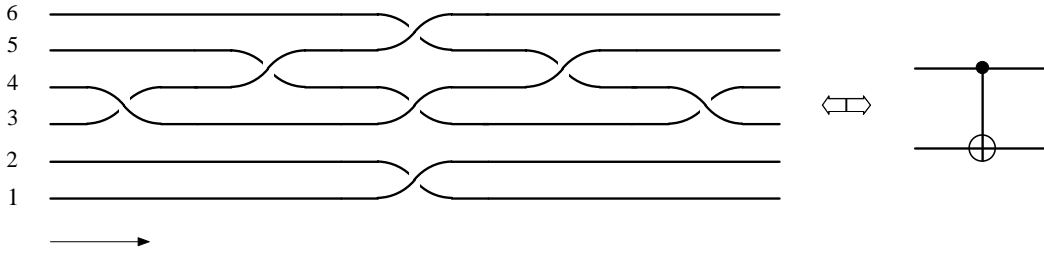


Fig. 16. The braid diagram for the Controlled-NOT gate executed by 7 elementary 6-quasi-particle braidings corresponding to Eq. (54). The symbol on the right is the standard quantum-computation notation for CNOT.

This is the first known construction of the Controlled-Z and Controlled-NOT gates entirely in terms of the braid matrices for 6 quasiholes in the Pfaffian TQC scheme, which certainly guarantees the exactness and topological protections of these gates.

Note that this construction of the CNOT gate is equivalent to the braid realization of the Bell matrix of Refs. [53,26]. The algebraic structure behind this Bell matrix, when it is used as a universal R matrix in the $R(T \otimes T) = (T \otimes T)R$ relations, giving rise to an exotic new bialgebra called S03, has been clarified in Ref. [54].

8.5 The Bravyi–Kitaev Controlled-Z gate precursor

For the sake of completeness and comparison we shall also describe the existing idea [29] to realize CZ by taking one quasihole, around two other, which suffers from the drawback that the resulting transformation has one extra minus sign and thus has to be supplemented by external operations in order to produce the CZ gate, see below. Consider, e.g., the quasihole with position η_1 , from qubit 1 transported adiabatically around the two quasiholes, with positions η_5 and η_6 , of qubit 2 (or, equivalently, taking the two quasiholes comprising qubit 2 around one quasihole of qubit 1) as shown on Fig. 17. This is obviously equivalent to first taking η_1

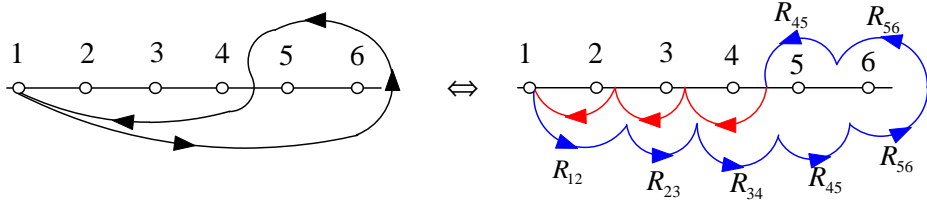


Fig. 17. The Controlled-Z gate precursor in terms of the monodromies $\widetilde{\text{CZ}} = R_{15}^2 R_{16}^2$.

around η_6 and then around η_5 so that this gate would be just the product of the two corresponding monodromies

$$\widetilde{\text{CZ}} = R_{15}^2 R_{16}^2 \simeq R_{12}^{-1} R_{23}^{-1} R_{34}^{-1} R_{45} R_{56}^2 R_{45} R_{34} R_{23} R_{12} = \begin{pmatrix} 1 & 0 & 0 & 0 \\ 0 & -1 & 0 & 0 \\ 0 & 0 & 1 & 0 \\ 0 & 0 & 0 & -1 \end{pmatrix}. \quad (55)$$

The second equality in Eq. (55) is just an equivalent representation which can be readoff from Fig. 17. We give for convenience also the explicit expression for R_{15}^2

$$R_{15}^2 = R_{12}^{-1} R_{23}^{-1} R_{34}^{-1} R_{45} R_{34} R_{23} R_{12} = e^{i\frac{\pi}{4}} \begin{pmatrix} 0 & 0 & 0 & 1 \\ 0 & 0 & -1 & 0 \\ 0 & 1 & 0 & 0 \\ -1 & 0 & 0 & 0 \end{pmatrix},$$

which together with Eq. (56) below can be used to compute $\widetilde{\text{CZ}}$ directly. The braid diagram for this realization of the CZ gate precursor is shown on Fig. 18. Now it is obvious that the gate we constructed in Eq. (55) differs from the CZ gate by having one more minus sign. The reason is that if the second qubit is in the state $|1\rangle$ the transport of the quasihole at η_1 will always produce a minus sign whatever the state of the first qubit (note that the two states which are multiplied by -1 by our gate (55) are exactly $|01\rangle$ and $|11\rangle$). The idea of Bravyi–Kitaev [29] is to

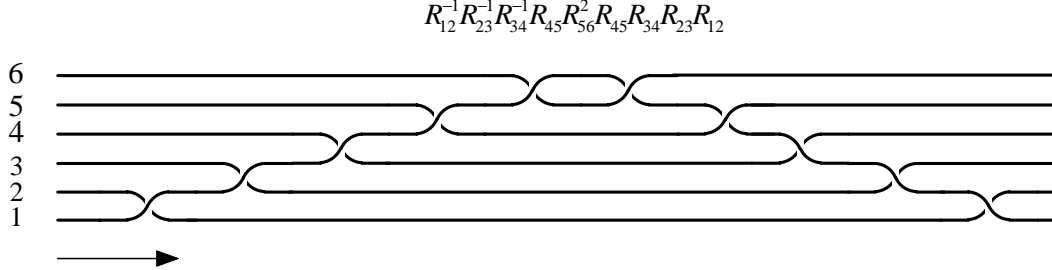


Fig. 18. The braid diagram for the monodromy-based Controlled-Z gate precursor.

split the first qubit into two 1/4-charge states only if this qubit is in the state $|1\rangle$ and then move the two quasiholes (at positions η_5 and η_6 in our case) forming the second qubit around the first qubit in order to execute this gate. This would remove the minus sign from the second row of $\widetilde{\text{CZ}}$ in Eq. (55) and, if successfully implemented, should give us a topologically protected Controlled-Z gate .

8.6 Realization of the Bravyi–Kitaev two-qubit gate g_3

One particular universal set of quantum gates, relevant for TQC with Pfaffian qubits, which has been proposed by Bravyi and Kitaev, is [29]

$$g_1 = \begin{pmatrix} 1 & 0 \\ 0 & e^{i\frac{\pi}{4}} \end{pmatrix}, \quad g_2 = \begin{pmatrix} 1 & 0 & 0 & 0 \\ 0 & 1 & 0 & 0 \\ 0 & 0 & 1 & 0 \\ 0 & 0 & 0 & -1 \end{pmatrix}, \quad g_3 = \frac{1}{\sqrt{2}} \begin{pmatrix} 1 & 0 & 0 & -i \\ 0 & 1 & -i & 0 \\ 0 & -i & 1 & 0 \\ -i & 0 & 0 & 1 \end{pmatrix}.$$

The two-qubit gate g_2 is identical with our Controlled-Z gate (51) implemented in a topologically protected manner by 6-quasiholes braidings. The single-qubit gate g_1 , known also as the $\pi/8$ gate T , has been realized in Ref. [29] as an unprotected gate, by bringing together the two quasiholes for a short period of time and then pulling them back, in which the exponential topological protection is lost.

In trying to construct the gate g_3 it would be instructive to compute first the monodromy R_{16}^2 as taking η_1 around η_6 . As is obvious from Fig. 19, this monodromy can be expressed in terms of the elementary 6-quasiholes exchanges⁶ (omitting the superscript (6) in the R -matrices) as

$$R_{16}^2 = R_{12}^{-1}R_{23}^{-1}R_{34}^{-1}R_{45}^{-1}R_{56}^2R_{45}R_{34}R_{23}R_{12} = \begin{pmatrix} 0 & 0 & 0 & 1 \\ 0 & 0 & 1 & 0 \\ 0 & 1 & 0 & 0 \\ 1 & 0 & 0 & 0 \end{pmatrix}. \quad (56)$$

⁶ note that the clockwise exchanges correspond to the inverse exchange matrices

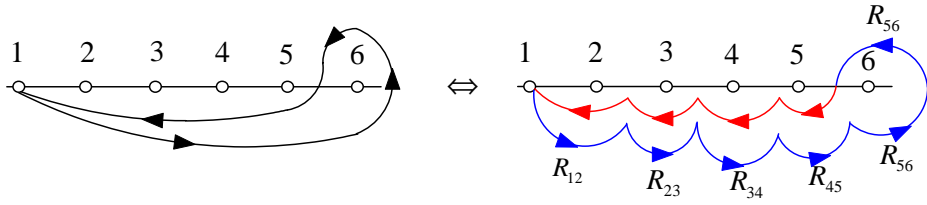


Fig. 19. The monodromy R_{16}^2 executed by taking η_1 around η_6 in a counter-clockwise direction.

Then the exchange R_{16} is just the “square-root” of Eq. (56), i.e.,

$$R_{16} = R_{12}^{-1} R_{23}^{-1} R_{34}^{-1} R_{45}^{-1} R_{56} R_{45} R_{34} R_{23} R_{12}. \quad (57)$$

The direct computation, using the explicit formulas, Eqs. (45), (46), (50), (47) and (48) for the elementary R matrices, shows that the two-qubit gate g_3 identical with R_{16} , i.e.,

$$R_{16} \simeq \frac{1}{\sqrt{2}} \begin{pmatrix} 1 & 0 & 0 & -i \\ 0 & 1 & -i & 0 \\ 0 & -i & 1 & 0 \\ -i & 0 & 0 & 1 \end{pmatrix} \equiv g_3.$$

The braid diagram for the realization of R_{16} is shown in Fig. 20.

$$R_{16} = R_{12}^{-1} R_{23}^{-1} R_{34}^{-1} R_{45}^{-1} R_{56} R_{45} R_{34} R_{23} R_{12}$$

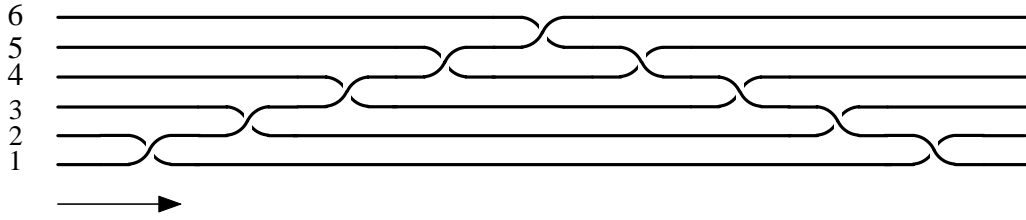


Fig. 20. Implementing the two-qubit gate g_3 by counter-clockwise exchange of the quasiholes with positions η_1 and η_6 .

Remark 2 It is worth stressing that the TQC scheme of Das Sarma *et al.* [28] is essentially based on the monodromy transformations of the multi-quasihole Pfaffian wave functions. The only exception is the Bravyi–Kitaev gate g_3 , which was proposed to be constructed schematically in Ref. [29] by braiding two among 4 quasiholes (not by braiding 6 quasiholes as it should be). Note, however, that as a two-qubit gate acting on Pfaffian qubits, g_3 must be constructed in terms of transformations of the 6-quasihole states, which has not been done in Ref. [29]. In particular, it is not clear from the 4-quasihole braiding construction of Ref. [29],

which two quasiholes among the 6 ones must be exchanged in order to obtain the gate g_3 , and whether this is at all possible. The first explicit results proving the usefulness of braidings for topological quantum computation with Pfaffian quasiholes have been obtained in Ref. [46] and Eq. (57) is the braiding implementation of g_3 .

Just for reference, and to demonstrate the importance⁷ of the choice of quasiholes to be exchanged, we note that in a similar way the exchange of η_2 with η_5 gives rise to the following matrix

$$R_{25} = R_{23}^{-1} R_{34}^{-1} R_{45} R_{34} R_{23} = \frac{e^{i\frac{\pi}{4}}}{\sqrt{2}} \begin{pmatrix} 1 & 0 & 0 & -i \\ 0 & 1 & i & 0 \\ 0 & i & 1 & 0 \\ -i & 0 & 0 & 1 \end{pmatrix}.$$

8.7 The non-demolition measurement gate

One of the quantum gates in the universal TQC schemes reviewed in Ref. [29] is executed by a non-demolition measurement of the total topological charge of two qubits. According to our construction of the two-qubit states this measurement is equivalent to the transformation

$$|00\rangle \rightarrow |00\rangle, \quad |01\rangle \rightarrow -|01\rangle, \quad |10\rangle \rightarrow -|10\rangle, \quad |11\rangle \rightarrow |01\rangle.$$

Therefore we can identify the non-demolition measurement gate with the monodromy matrix corresponding to the adiabatic transport of η_3 around η_4

$$\left(R_{34}^{(6)}\right)^2 = \begin{pmatrix} 1 & 0 & 0 & 0 \\ 0 & -1 & 0 & 0 \\ 0 & 0 & -1 & 0 \\ 0 & 0 & 0 & 1 \end{pmatrix} \simeq Z_1 Z_2,$$

where $Z_1 = \left(R_{12}^{(6)}\right)^2$ and $Z_2 = \left(R_{56}^{(6)}\right)^2$ are the Pauli Z -gates over the first and second qubits, respectively. While the non-demolition measurement of the total topological charge might happen to be noisy, the implementation of the above quantum gate as a 6-quasiholes state monodromy is completely protected by topology.

⁷ note that R_{25} and R_{16} are not equivalent as quantum operations

8.8 The two-qubit swap gate

Once we now how to construct the CNOT gate it is straight forward to obtain the two-qubit Swap gate in terms of three CNOTs [24] as shown in the top line of Fig. 21. Here we shall demonstrate that it is possible to implement the Swap gate with 15 elementary exchanges. The bottom line of Fig. 21 shows how to express

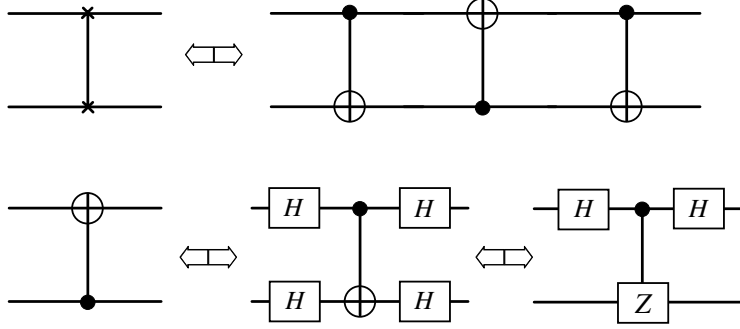


Fig. 21. The two-qubit SWAP gate realized by three CNOT's

the swapped CNOT in terms of the CZ and Hadamard gates. It turns out that in this circuit H is essentially equivalent to $R_{23}^{(4)}$ so that substituting $(H \otimes \mathbb{I}_2) \simeq R_{23}^{(6)}$ and $(\mathbb{I}_2 \otimes H) \simeq R_{45}^{(6)}$, as well as using Eq. (51) for CZ, we finally obtain

$$\begin{aligned}
 \text{Swap} &\simeq (\mathbb{I}_2 \otimes H) \text{ CZ } (\mathbb{I}_2 \otimes H) \text{ } (H \otimes \mathbb{I}_2) \text{ CZ } (H \otimes \mathbb{I}_2) \text{ } (\mathbb{I}_2 \otimes H) \text{ CZ } (\mathbb{I}_2 \otimes H) \\
 &\simeq R_{45} R_{34}^{-1} R_{12} R_{56} R_{45} R_{23} R_{34}^{-1} R_{12} R_{56} R_{23} R_{45} R_{34}^{-1} R_{12} R_{56} R_{45} \\
 &= i \begin{pmatrix} 1 & 0 & 0 & 0 \\ 0 & 0 & 1 & 0 \\ 0 & 1 & 0 & 0 \\ 0 & 0 & 0 & 1 \end{pmatrix}. \tag{58}
 \end{aligned}$$

9 Universal TQC scheme based on the Hadamard gate H , phase gate S , CNOT and Toffoli gate

One of the standard universal set of gates, which could be used for universal quantum computation, includes the Hadamard gate H , the phase gate S , the two-qubit CNOT gate and the Toffoli gate, which is a three-qubit Controlled-Controlled-NOT (CCNOT) gate [24]. In order to execute three-qubit gates, such as the Toffoli and Fredkin gates, we need to consider a system with 8 quasiholes, whose Hilbert subspace of states (for fixed positions of the quasiholes) has dimension $2^{\frac{8}{2}-1} = 8$. Here we shall assume that the third qubit is defined by 2 more quasiholes at positions η_7

and η_8 as shown on Fig. 22. Then the three-qubit basis can be written in terms of the Ising spin fields as follows

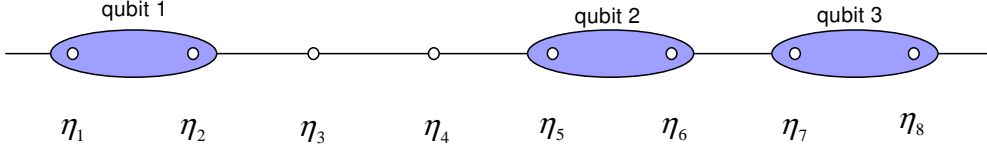


Fig. 22. Three qubits constructed from 8 quasiholes

$$\begin{aligned}
 |000\rangle &\equiv \langle \sigma_+ \sigma_+ \sigma_+ \sigma_+ \sigma_+ \sigma_+ \sigma_+ \sigma_+ \rangle, & |001\rangle &\equiv \langle \sigma_+ \sigma_+ \sigma_+ \sigma_- \sigma_+ \sigma_+ \sigma_+ \sigma_- \rangle, \\
 |010\rangle &\equiv \langle \sigma_+ \sigma_+ \sigma_+ \sigma_- \sigma_+ \sigma_- \sigma_+ \sigma_+ \rangle, & |011\rangle &\equiv \langle \sigma_+ \sigma_+ \sigma_+ \sigma_+ \sigma_+ \sigma_- \sigma_+ \sigma_- \rangle, \\
 |100\rangle &\equiv \langle \sigma_+ \sigma_- \sigma_+ \sigma_- \sigma_+ \sigma_+ \sigma_+ \sigma_+ \rangle, & |101\rangle &\equiv \langle \sigma_+ \sigma_- \sigma_+ \sigma_+ \sigma_+ \sigma_+ \sigma_+ \sigma_- \rangle, \\
 |110\rangle &\equiv \langle \sigma_+ \sigma_- \sigma_+ \sigma_+ \sigma_+ \sigma_- \sigma_+ \sigma_+ \rangle, & |111\rangle &\equiv \langle \sigma_+ \sigma_- \sigma_+ \sigma_- \sigma_+ \sigma_- \sigma_+ \sigma_- \rangle. \tag{59}
 \end{aligned}$$

Now the fermion parity conservation requires that

$$e_3 e_4 = e_1 e_2 e_5 e_6 e_7 e_8,$$

which reduces the number of independent states to from 16 to 8. Although we have chosen the quasiholes at η_3 and η_4 in such a way to preserve the fermion parity, any other choice of the positions of quasiholes representing the three qubits would be equivalent to Eq. (59) because the braid matrices for the elementary exchanges would be just conjugated by an element of the braid group, and the Artin relations (37) are invariant under conjugation.

9.1 Exchange matrices for 8 quasiholes

Using the fusion rules (27) of the non-Abelian quasiholes we can express the exchange matrices for 8 quasiholes recursively in terms of those for 6 quasiholes as follows:

$$R_{12}^{(8)} = \text{diag}(1, 1, 1, 1, i, i, i, i) = R_{12}^{(6)} \otimes \mathbb{I}_2, \tag{60}$$

$$R_{23}^{(8)} = \frac{e^{i\frac{\pi}{4}}}{\sqrt{2}} \begin{pmatrix} 1 & 0 & 0 & 0 & -i & 0 & 0 & 0 \\ 0 & 1 & 0 & 0 & 0 & -i & 0 & 0 \\ 0 & 0 & 1 & 0 & 0 & 0 & -i & 0 \\ 0 & 0 & 0 & 1 & 0 & 0 & 0 & -i \\ -i & 0 & 0 & 0 & 1 & 0 & 0 & 0 \\ 0 & -i & 0 & 0 & 0 & 1 & 0 & 0 \\ 0 & 0 & -i & 0 & 0 & 0 & 1 & 0 \\ 0 & 0 & 0 & -i & 0 & 0 & 0 & 1 \end{pmatrix} = R_{23}^{(6)} \otimes \mathbb{I}_2, \tag{61}$$

$$R_{34}^{(8)} = \text{diag}(1, i, i, 1, i, 1, 1, i), \quad (62)$$

$$R_{45}^{(8)} = \frac{e^{i\frac{\pi}{4}}}{\sqrt{2}} \begin{pmatrix} 1 & 0 & -i & 0 & 0 & 0 & 0 & 0 \\ 0 & 1 & 0 & -i & 0 & 0 & 0 & 0 \\ -i & 0 & 1 & 0 & 0 & 0 & 0 & 0 \\ 0 & -i & 0 & 1 & 0 & 0 & 0 & 0 \\ 0 & 0 & 0 & 0 & 1 & 0 & -i & 0 \\ 0 & 0 & 0 & 0 & 0 & 1 & 0 & -i \\ 0 & 0 & 0 & 0 & -i & 0 & 1 & 0 \\ 0 & 0 & 0 & 0 & 0 & -i & 0 & 1 \end{pmatrix} = R_{45}^{(6)} \otimes \mathbb{I}_2, \quad (63)$$

$$R_{56}^{(8)} = \text{diag}(1, 1, i, i, 1, 1, i, i) = R_{56}^{(6)} \otimes \mathbb{I}_2, \quad (64)$$

$$R_{67}^{(8)} = \frac{e^{i\frac{\pi}{4}}}{\sqrt{2}} \begin{pmatrix} 1 & 0 & 0 & -i & 0 & 0 & 0 & 0 \\ 0 & 1 & -i & 0 & 0 & 0 & 0 & 0 \\ 0 & -i & 1 & 0 & 0 & 0 & 0 & 0 \\ -i & 0 & 0 & 1 & 0 & 0 & 0 & 0 \\ 0 & 0 & 0 & 0 & 1 & 0 & 0 & -i \\ 0 & 0 & 0 & 0 & 0 & 1 & -i & 0 \\ 0 & 0 & 0 & 0 & 0 & -i & 1 & 0 \\ 0 & 0 & 0 & 0 & -i & 0 & 0 & 1 \end{pmatrix}, \quad (65)$$

$$R_{78}^{(8)} = \text{diag}(1, i, 1, i, 1, i, 1, i) = \mathbb{I}_2 \otimes R_{56}^{(6)}. \quad (66)$$

It is not difficult to check that the exchange matrices (60), (61), (62), (63), (64), (65) and (66) satisfy the Artin relations (37) for the braid group \mathcal{B}_8 . Again, the order of the representation of the braid group \mathcal{B}_8 and its monodromy subgroup can be obtained by Dimino's algorithm [50] to be

$$|\text{Image}(\mathcal{B}_8)| = 5160960, \quad |\text{Image}(\mathcal{M}_8)| = 128.$$

As an illustration of the derivation of the 8-quasihole exchange matrices, let us compute the last row of $R_{67}^{(8)}$, i.e., we consider the transformation of the state $|111\rangle$ when we exchange η_6 with η_7 . Because the state of the second and the third qubits is independent of the quasiholes at η_1 and η_2 , we could fuse $\eta_1 \rightarrow \eta_2$ obtaining in this way a 6-quasihole state whose braiding properties are already known. Indeed, using the OPE (27) we find

$$\begin{aligned} |111\rangle &\underset{\eta_1 \rightarrow \eta_2}{\simeq} \sqrt{\frac{\eta_{12}}{2}} \langle \psi(\eta_2) \sigma_+(\eta_3) \sigma_-(\eta_4) \sigma_+(\eta_5) \sigma_-(\eta_6) \sigma_+(\eta_7) \sigma_-(\eta_8) \rangle \\ &\underset{\eta_2 \rightarrow \eta_3}{\simeq} \sqrt{\frac{\eta_{12}}{2}} \sqrt{\frac{1}{2\eta_{23}}} \langle \sigma_-(\eta_3) \sigma_-(\eta_4) \sigma_+(\eta_5) \sigma_-(\eta_6) \sigma_+(\eta_7) \sigma_-(\eta_8) \rangle \simeq |01\rangle \end{aligned}$$

where we used the OPE [45] $\psi(\eta_2) \sigma_{e_3}(\eta_3) \simeq (2\eta_{23})^{-1/2} \sigma_{-e_3}(\eta_3)$, for $\eta_2 \rightarrow \eta_3$, and the identity $\langle \sigma_- \sigma_- \sigma_+ \sigma_- \sigma_+ \sigma_- \rangle \simeq \langle \sigma_+ \sigma_+ \sigma_+ \sigma_- \sigma_+ \sigma_- \rangle \equiv |01\rangle$. It is now obvious that the exchange of η_6 with η_7 in the three-qubit state $|111\rangle$ is equivalent to

the exchange of the fifth and sixth quasiholes in the state $|01\rangle$ so that, taking $R_{45}^{(6)}$ from Eq. (47), we obtain

$$\begin{aligned}
|111\rangle &\xrightarrow{R_{45}^{(6)}} \frac{e^{i\frac{\pi}{4}}}{\sqrt{2}} \sqrt{\frac{\eta_{12}}{2}} \sqrt{\frac{1}{2\eta_{23}}} (-i|00\rangle + |01\rangle) \\
&= \frac{e^{i\frac{\pi}{4}}}{\sqrt{2}} \sqrt{\frac{\eta_{12}}{2}} \sqrt{\frac{1}{2\eta_{23}}} (-i\langle\sigma_+(\eta_3)\sigma_+(\eta_4)\sigma_+(\eta_5)\sigma_+(\eta_6)\sigma_+(\eta_7)\sigma_+(\eta_8)\rangle \\
&+ \langle\sigma_+(\eta_3)\sigma_+(\eta_4)\sigma_+(\eta_5)\sigma_-(\eta_6)\sigma_+(\eta_7)\sigma_-(\eta_8)\rangle) \\
&\stackrel{\eta_2 \rightarrow \eta_3}{\simeq} \frac{e^{i\frac{\pi}{4}}}{\sqrt{2}} \sqrt{\frac{\eta_{12}}{2}} (-i\langle\psi(\eta_2)\sigma_-(\eta_3)\sigma_+(\eta_4)\sigma_+(\eta_5)\sigma_+(\eta_6)\sigma_+(\eta_7)\sigma_+(\eta_8)\rangle \\
&+ \langle\psi(\eta_2)\sigma_-(\eta_3)\sigma_+(\eta_4)\sigma_+(\eta_5)\sigma_-(\eta_6)\sigma_+(\eta_7)\sigma_-(\eta_8)\rangle) \\
&\stackrel{\eta_1 \rightarrow \eta_2}{\simeq} \frac{e^{i\frac{\pi}{4}}}{\sqrt{2}} (-i\langle\sigma_+(\eta_1)\sigma_-(\eta_2)\sigma_+(\eta_3)\sigma_-(\eta_4)\sigma_+(\eta_5)\sigma_+(\eta_6)\sigma_+(\eta_7)\sigma_+(\eta_8)\rangle \\
&+ \langle\sigma_+(\eta_1)\sigma_-(\eta_2)\sigma_+(\eta_3)\sigma_-(\eta_4)\sigma_+(\eta_5)\sigma_-(\eta_6)\sigma_+(\eta_7)\sigma_-(\eta_8)\rangle) \\
&= \frac{e^{i\frac{\pi}{4}}}{\sqrt{2}} (-i|100\rangle + |111\rangle), \tag{67}
\end{aligned}$$

which exactly reproduces the last row of $R_{67}^{(8)}$. In the above derivation we restored the 8-quasiholes states using the same OPEs for $\eta_2 \rightarrow \eta_3$ and $\eta_1 \rightarrow \eta_2$, however in reverse, as well as used the identity $\sigma_-(\eta_3)\sigma_+(\eta_4) \simeq \sigma_+(\eta_3)\sigma_-(\eta_4)$.

Remark 3 Due to the specifics of the braid group representation, it may not be always possible to represent exactly the single- and two-qubit gates in the three-qubit basis (59). Indeed, the 6-quasiholes exchange matrix $R_{34}^{(6)}$, defined in Eq. (50), is not a factorized tensor product of the exchange matrices for 4 quasiholes, rather it contains the built-in CZ matrix (51). Therefore some tensor products, which are trivial otherwise, might not be constructed directly in terms of the elementary exchange matrices for 8 quasiholes. One consequence of this peculiarity is that some one-qubit and two-qubit gates would be easier realizable in the three-qubit basis (59) in terms of elementary 8-quasiholes exchange matrices, however, up to a pair of extra minus signs, see Sect. 9.2. While the exact construction of the one-qubit and two-qubit gates would require more work, their simplified versions might be sufficient in most cases.

9.2 Embedding of one-qubit and two-qubit gates into a three-qubit system

The three one-qubit phase gates are directly expressed as single elementary 8-quasiholes exchange matrices, i.e.,

$$S_1 \equiv S \otimes \mathbb{I}_4 = R_{12}^{(8)}, \quad S_2 \equiv \mathbb{I}_2 \otimes S \otimes \mathbb{I}_2 = R_{56}^{(8)}, \quad S_3 \equiv \mathbb{I}_4 \otimes S = R_{78}^{(8)}.$$

The first one-qubit Hadamard gate can be constructed exactly in terms of the exchange matrices for 8 quasiholes by (skipping the superscript “(8)” of R)

$$H_1 = H \otimes \mathbb{I}_4 \simeq R_{12}^{-1} R_{23}^{-1} R_{12}^{-1} = \frac{e^{-i\frac{\pi}{4}}}{\sqrt{2}} \begin{pmatrix} 1 & 0 & 0 & 0 & 1 & 0 & 0 & 0 \\ 0 & 1 & 0 & 0 & 0 & 1 & 0 & 0 \\ 0 & 0 & 1 & 0 & 0 & 0 & 1 & 0 \\ 0 & 0 & 0 & 1 & 0 & 0 & 0 & 1 \\ 1 & 0 & 0 & 0 & -1 & 0 & 0 & 0 \\ 0 & 1 & 0 & 0 & 0 & -1 & 0 & 0 \\ 0 & 0 & 1 & 0 & 0 & 0 & -1 & 0 \\ 0 & 0 & 0 & 1 & 0 & 0 & 0 & -1 \end{pmatrix}, \quad (68)$$

while the second Hadamard gate could be constructed as follows

$$H_2 \simeq \mathbb{I}_2 \otimes H \otimes \mathbb{I}_2 \simeq R_{56}^{-1} R_{45}^{-1} R_{56}^{-1} = \frac{e^{-i\frac{\pi}{4}}}{\sqrt{2}} \begin{pmatrix} 1 & 0 & 1 & 0 & 0 & 0 & 0 & 0 \\ 0 & 1 & 0 & 1 & 0 & 0 & 0 & 0 \\ 1 & 0 & -1 & 0 & 0 & 0 & 0 & 0 \\ 0 & 1 & 0 & -1 & 0 & 0 & 0 & 0 \\ 0 & 0 & 0 & 0 & 1 & 0 & 1 & 0 \\ 0 & 0 & 0 & 0 & 0 & 1 & 0 & 1 \\ 0 & 0 & 0 & 0 & 1 & 0 & -1 & 0 \\ 0 & 0 & 0 & 0 & 0 & 1 & 0 & -1 \end{pmatrix}. \quad (69)$$

The third Hadamard gate could also be reproduced up to some swapping by

$$H_3 = \mathbb{I}_4 \otimes H \simeq R_{78}^{-1} R_{45}^{-1} R_{56}^{-1} R_{67}^{-1} R_{56}^{-1} R_{45}^{-1} R_{78}^{-1} \\ = \frac{-e^{i\frac{\pi}{4}}}{\sqrt{2}} \begin{pmatrix} 1 & 1 & 0 & 0 & 0 & 0 & 0 & 0 \\ 1 & -1 & 0 & 0 & 0 & 0 & 0 & 0 \\ 0 & 0 & -1 & 1 & 0 & 0 & 0 & 0 \\ 0 & 0 & 1 & 1 & 0 & 0 & 0 & 0 \\ 0 & 0 & 0 & 0 & 1 & 1 & 0 & 0 \\ 0 & 0 & 0 & 0 & 1 & -1 & 0 & 0 \\ 0 & 0 & 0 & 0 & 0 & 0 & -1 & 1 \\ 0 & 0 & 0 & 0 & 0 & 0 & 1 & 1 \end{pmatrix}. \quad (70)$$

It might be useful to give also the realization of the single-qubit NOT gates: $X_1 \equiv X \otimes \mathbb{I}_4 = R_{23}^2$, $X_2 \equiv \mathbb{I}_2 \otimes X \otimes \mathbb{I}_2 = R_{45}^2$ and $X_3 \equiv \mathbb{I}_4 \otimes X = R_{45}^2 R_{67}^2$.

We should stress again that the topological entanglement between the qubits mentioned in Sect. 8.3 leads to serious difficulties for efficient embedding of the one-qubit and two-qubit gates in three-qubit systems. For example, the NOT gate X_3 acting on the third qubit has a different structure than just a tensor product of the exchange matrix producing the single-qubit X gate. Similarly, the Hadamard gates acting on the first and second qubits have slightly different structures from their

single-qubit counterpart H , while that acting on the third qubit cannot even be obtained exactly with the same number of elementary exchanges as H . This seems to be a common problem arising in all TQC schemes using non-Abelian anyons in FQH systems, whose general solution is still missing. Moreover, it appears that the two-qubit Controlled-NOT gates in a three-qubit systems cannot be directly constructed in the three-qubit basis (59) because of the topological entanglement between the two qubits and the third one. This requires more work and will be reported elsewhere. Just for reference, we give a simple implementation of a three-qubit operation which is very close to $\text{CNOT}_2 = \mathbb{I}_2 \otimes \text{CNOT}$

$$\begin{aligned} \widetilde{\text{CNOT}}_2 &\simeq \mathbb{I}_2 \otimes \text{CNOT} \simeq R_{12}^{-1} R_{56} \widetilde{\text{SWAP}}_2 R_{36} R_{45} \widetilde{\text{SWAP}}_2 \\ &= \begin{pmatrix} 1 & 0 & 0 & 0 & 0 & 0 & 0 & 0 \\ 0 & 1 & 0 & 0 & 0 & 0 & 0 & 0 \\ 0 & 0 & 0 & 1 & 0 & 0 & 0 & 0 \\ 0 & 0 & 1 & 0 & 0 & 0 & 0 & 0 \\ 0 & 0 & 0 & 0 & 0 & 1 & 0 & 0 \\ 0 & 0 & 0 & 0 & 1 & 0 & 0 & 0 \\ 0 & 0 & 0 & 0 & 0 & 0 & 1 & 0 \\ 0 & 0 & 0 & 0 & 0 & 0 & 0 & 1 \end{pmatrix}, \end{aligned} \quad (71)$$

where $R_{36} = R_{56}^{-1} R_{45}^{-1} R_{34}^{-1} R_{45} R_{56}$ and the gate $\widetilde{\text{SWAP}}_2$ is defined below.

The two-qubit SWAP gates can be simply realized by braiding in the three-qubit basis (59) (up to overall phases and pairs of extra minus signs) by

$$\begin{aligned} \widetilde{\text{SWAP}}_1 &\simeq \text{SWAP} \otimes \mathbb{I}_2 \simeq R_{45} R_{56}^{-1} R_{34}^{-1} R_{45} R_{23} R_{34}^{-1} R_{12}^{-1} R_{23} R_{45} R_{56}^{-1} R_{34}^{-1} R_{45} \\ &= \begin{pmatrix} -1 & 0 & 0 & 0 & 0 & 0 & 0 & 0 \\ 0 & -1 & 0 & 0 & 0 & 0 & 0 & 0 \\ 0 & 0 & 0 & 0 & 1 & 0 & 0 & 0 \\ 0 & 0 & 0 & 0 & 0 & -1 & 0 & 0 \\ 0 & 0 & 1 & 0 & 0 & 0 & 0 & 0 \\ 0 & 0 & 0 & -1 & 0 & 0 & 0 & 0 \\ 0 & 0 & 0 & 0 & 0 & 0 & 1 & 0 \\ 0 & 0 & 0 & 0 & 0 & 0 & 0 & 1 \end{pmatrix} \\ \widetilde{\text{SWAP}}_2 &\simeq \mathbb{I}_2 \otimes \text{SWAP} \simeq R_{67} R_{78}^{-1} R_{56}^{-1} R_{67} = \begin{pmatrix} -1 & 0 & 0 & 0 & 0 & 0 & 0 & 0 & 0 \\ 0 & 0 & 1 & 0 & 0 & 0 & 0 & 0 & 0 \\ 0 & 1 & 0 & 0 & 0 & 0 & 0 & 0 & 0 \\ 0 & 0 & 0 & 1 & 0 & 0 & 0 & 0 & 0 \\ 0 & 0 & 0 & 0 & -1 & 0 & 0 & 0 & 0 \\ 0 & 0 & 0 & 0 & 0 & 0 & 0 & 1 & 0 \\ 0 & 0 & 0 & 0 & 0 & 0 & 1 & 0 & 0 \\ 0 & 0 & 0 & 0 & 0 & 0 & 0 & 0 & 1 \end{pmatrix} \end{aligned} \quad (72)$$

The Swap gates turn out to be very important because they can be used to construct gates acting on one of the qubits in terms of similar gates acting on another qubit. For example, the CNOT gate acting on the first and the third qubits can be expressed in terms of the CNOT acting on the first and the second qubit plus two gates SWAP_2 . The extra minus signs appearing in some of the three-qubit opera-

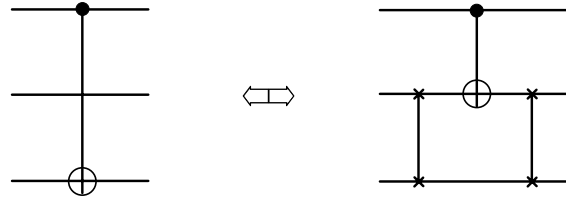


Fig. 23. The CNOT acting on qubits 1 and 3 expressed in terms of $\text{CNOT} \otimes \mathbb{I}_2$, which is the CNOT gate acting on qubits 1 and 2, and two gates $\mathbb{I}_2 \otimes \text{SWAP}$.

tions are not an innocent thing, because they may have different properties from the standard gates. However, it appears that in many cases these simplified gates, which are much simpler to construct, can be used instead of the standard once.

9.3 Toffoli gate constructed in terms of the Controlled-S gate and CNOT

One way to construct the Toffoli gate is to use the Controlled-Controlled-Z (CCZ) gate conjugated by the single-qubit Hadamard gate H_3 , acting on the target qubit, whose exact construction in terms of the 8-quasiholes braid matrices is given in Eq. (70), i.e.,

$$\text{CCNOT} = (\mathbb{I}_2 \otimes \mathbb{I}_2 \otimes H) \text{ CCZ} (\mathbb{I}_2 \otimes \mathbb{I}_2 \otimes H), \quad (73)$$

where $\text{CCZ} = \text{diag}(1, 1, 1, 1, 1, 1, 1, -1)$. On the other hand, because the Pauli Z gate is just the square of the phase gate S , the CCZ gate can be constructed [24,37] with the help of the Controlled-S (CS) gate and its conjugate as shown on Fig. 24. Now the problem is how to realize the CS gate, which is defined in the basis (42)

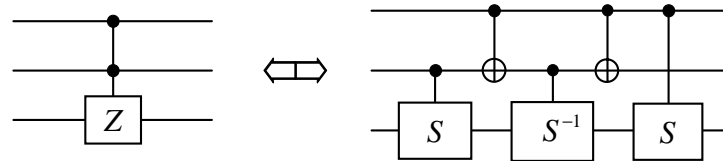


Fig. 24. The Controlled-Controlled-Z gate realized by the Controlled-S gate and CNOT.

$$\text{CS} = \begin{pmatrix} 1 & 0 & 0 & 0 \\ 0 & 1 & 0 & 0 \\ 0 & 0 & 1 & 0 \\ 0 & 0 & 0 & i \end{pmatrix}.$$

Obviously CS cannot be expressed directly as a product of 6-quasihole exchange matrices because $\det \text{CS} = i$, while $\det(R_{a,a+1}^{(6)}) = -1$. It can be realized with the help of the $\pi/8$ gate T as shown on Fig. 25, which demonstrates that the use of the Toffoli gate is equivalent to the use of T . However, we might want to avoid using the

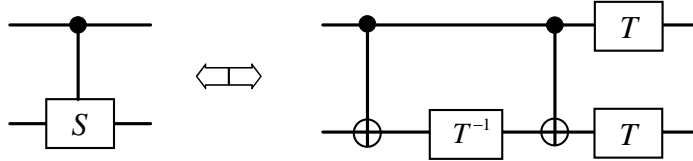


Fig. 25. The Controlled-S gate in terms of the $\pi/8$ gate T and CNOT.

$\pi/8$ gate. Instead, we could construct a braid-group based CS precursor, in terms of the braid matrix R_{56} defined in Eq. (48), and supplement it by the Bravyi–Kitaev condition that the first qubit is split into two $1/4$ -charge quasiholes only if it is in the state $|1\rangle$, just like in the case of the Bravyi–Kitaev CZ precursor discussed in Sect. 8.5. In this case, however, exchanging the quasiholes with positions η_5 and η_6 with η_1 we might obtain 1 on the second row of the diagonal matrix (48) instead of i , which is precisely the CS gate we want. The main advantage of this idea is that it can be realized with standard braiding, plus some external procedure, which might possibly provide topologically protected Controlled-S gate and Toffoli gates.

9.4 Toffoli gate constructed by a braid-group based Controlled-Controlled-Z gate precursor

Because of the relation (73) between the Toffoli gate and CCZ we can try to implement the Toffoli gate even more directly. Indeed, the construction of the CZ gate in Eq. (51) presents another possibility to realize the CCZ gate using as a braid-group based precursor the tensor product $\text{CZ} \otimes \mathbb{I}_2$ or, even more conveniently, by using the related diagonal matrix, obtained by multiplying the diagonal exchange matrices for 8 quasiholes,

$$\widetilde{\text{CCZ}} \equiv R_{12}^{(8)} R_{34}^{(8)} R_{56}^{(8)} R_{78}^{(8)} \simeq \text{diag}(-1, 1, 1, 1, 1, 1, 1, -1) \quad (74)$$

and apply again the Bravyi–Kitaev construction that the first qubit is split into two charge- $1/4$ quasiholes only if it is in the state $|1\rangle$ in order to remove the minus sign

on the first row. This is precisely the same situation as the proposed CZ precursor in Ref. [29] where the Bravyi–Kitaev construction removing the minus sign on the second row of their gate g_2 is believed to be realizable by tilted interferometry in planar geometry.

The tilted interferometry realization of the Bravyi–Kitaev construction [29] could eventually provide us with a topologically protected CCZ gate, hence, with a universal set of topologically protected gates that are sufficient for universal quantum computation with Pfaffian qubits.

10 Discussion

In this paper we explicitly implemented all single-qubit gates in the Pfaffian TQC scheme, except for the $\pi/8$ one, in terms of 4-quasihole braidings, as well as the two-qubit Controlled-Z and CNOT gates in terms of 6-quasihole braidings. These gates, which are known to form a Clifford group, are realized in a completely topologically protected way because of the topological nature of the braid operations in the FQH liquids. This work is an extension of the topological quantum computation scheme of Ref. [28] using pairs of Pfaffian quasiholes localized on antidots to construct elementary qubits and execute logical NOT on them. While the original TQC scheme of Ref. [28] used only monodromy transformations to realize quantum gates, we, for the first time, exploited explicitly quasihole braiding in the Pfaffian FQH state to construct the single-qubit Hadamard gate H , the phase gate S and the CNOT gate. Although the Gottesmann–Knill theorem says that any circuit based only on the Clifford group gates could be efficiently simulated on a (probabilistic) classical computer these gates do play a crucial role in quantum computation, especially in the error-correcting algorithms [24].

Due to the topological entanglement between the separate qubits realized by non-Abelian anyons in FQH systems some difficulties arise when trying to embed the one-qubit and two-qubit gates into systems with more qubits. This makes the embedding of Clifford gates non-trivial and requires more work.

For implementing three-qubit gates such as the Toffoli and Fredkin gates [24], in the Pfaffian TQC scheme, we considered Pfaffian wave functions with 8-quasiholes, in which case the topological degeneracy of the space of correlation functions is 8 [12,39]. We derived explicitly the braid matrices for the elementary 8-quasiholes exchanges, which serve as building blocks for constructing all three-qubit gates. More work in this direction, including eventually the topologically protected construction of the Toffoli gate would be reported elsewhere.

To conclude, let us make some remarks about the possible observation of the non-Abelian statistics. We believe that in order to observe the Pfaffian phase at $v = 5/2$

one should perform the experiment at temperature below 15 mK. The point is that there might exists another incompressible Abelian phase, which was called the Extended Pfaffian (EPf) state [33], that could also be realized at $v = 5/2$. Perhaps the most observable difference between the two phases is in the electric charge of their quasiparticles: $1/4$ for the Pfaffian and $1/2$ for the EPf. The EPf phase was obtained mathematically by a local chiral algebra extension of the Pfaffian state and satisfies all conditions necessary for an incompressible quantum Hall state [33]. The motivation for introducing this new state is that there is a persistent unexplained kink around $T_c = 15$ mK observed in the thermal activation experiment [55] showing two different slopes that presumably correspond to two different gaps below and above the critical temperature. Analyzing the edge states CFT it has been proposed in Ref. [33] a possible explanation of the kink in terms of a finite temperature two-step phase transition between the Pfaffian and the EPf state involving an intermediate compressible state of composite fermions. Here is a brief description of the process (see Sect. 9 in Ref. [33] for more details): at low temperature the system is definitely in the Pfaffian phase, as the numerical calculations suggest. As temperature increases to about $1/2$ of the Pfaffian-phase gap, which was estimated to be about 33 mK (for the sample of Ref. [55]), the system becomes more and more compressible (look at the behavior of the free energy on the edge, Fig. 5 in Ref. [33]) leading to a II-nd order phase transition to the compressible state of composite fermions (which has the same topological structure like the Pfaffian state but having at the same time the \mathbb{Z}_2 symmetry of the EPf state that is broken spontaneously in the Pfaffian phase). Immediately after that, as temperature continues to increase, there is a I-st order phase transition to the EPF state which is expected to have a higher gap than the Pfaffian state.

Acknowledgements

I thank Ivan Todorov, Ady Stern, Valentina Petkova, Chetan Nayak, Lyudmil Hadjiivanov and Michael Geller for many helpful discussions. This work has been partially supported by the FP5-EUCLID Network Program of the European Commission under Contract No. HPRN-CT-2002-00325 and by the Bulgarian National Council for Scientific Research under Contract No. F-1406.

A Binomial series expansion of the 4-pt function and analytic continuation

In this appendix we shall give some details about the analytic continuation of the function (19), which might be necessary for the understanding of the results of Sect. 3. Using the standard complex analysis notion [56] of a branching point as a multi-valued isolated singular point, we consider a punctured neighborhood of

the branching point, denoted as U' in which we would like to continue the element (U, f) of the function (19) from the simply-connected sub-domain $U \subset U'$ along any path. For example, for the branching point at $z = 0$ we can choose

$$U' = \{z \mid 0 < |z| < 1\}, \quad U = \{z \mid |z - 1/2| < 1/2\},$$

as shown on Fig. A.1. Then the analytic continuation along the contour

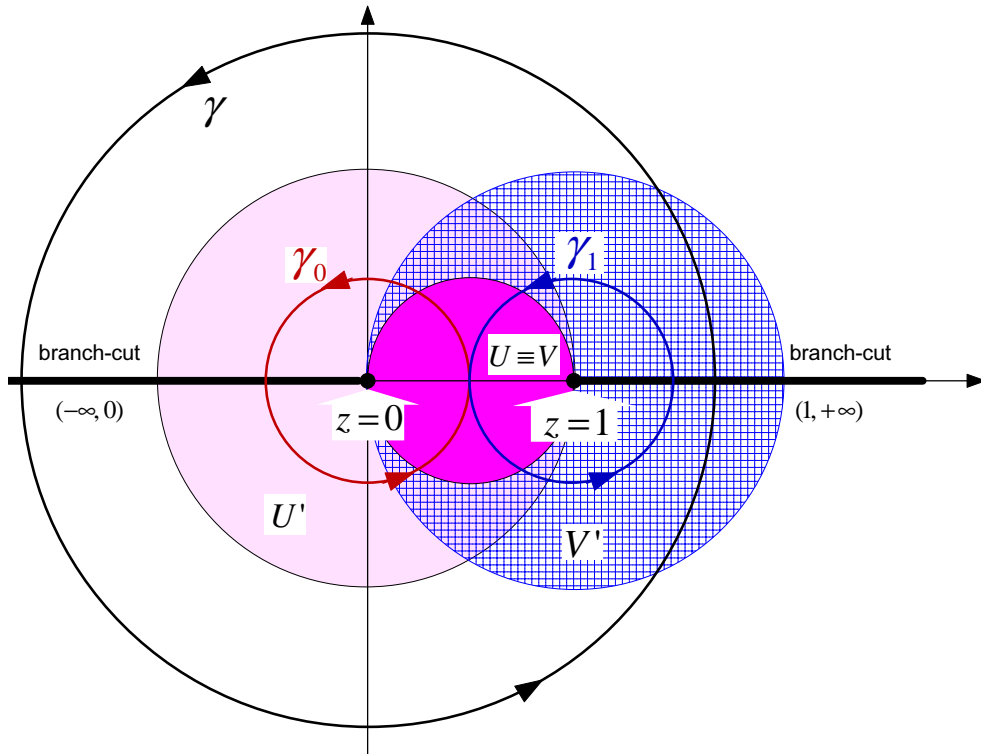


Fig. A.1. (Color online). Domains and contours for the different values of $|z|$ used for the analytic continuation and binomial series expansion

$$\gamma_0 = \left\{ z \mid z = \frac{1}{2}e^{it}, \quad 0 \leq t \leq 2\pi \right\} \quad (\text{A.1})$$

changes the sign in front of the inner root but not the one of the outer root because γ_0 does not encircle $z = 1$. This can be verified directly by using the (fractional powers) Laurent expansion, which in this case can be obtained by the binomial series expansion

$$(1+x)^\alpha = \sum_{n=0}^{\infty} \frac{\Gamma(\alpha+1)}{\Gamma(n+1)\Gamma(\alpha+1-n)} x^n, \quad |x| < 1$$

applied for $\alpha = 1/2$. Using the defining Γ function property $\Gamma(z) = (z-1)\Gamma(z-1)$, we get

$$\sqrt{1 \pm \sqrt{z}} = \left(1 \pm \frac{1}{2}\sqrt{z} - \frac{1}{8}z \pm \frac{1}{16}z\sqrt{z} - \dots \right), \quad z \in U'. \quad (\text{A.2})$$

That is why $\sqrt{1 \pm \sqrt{z}} \rightarrow \sqrt{1 \mp \sqrt{z}}$, for $|z| < 1$, when continuing $z \rightarrow e^{2\pi i}z$ along any contour in U' , which is homotopic to (A.1).

For the branching point at $z = 1$, on the other hand, we consider the domains V' and V shown again on Fig. A.1 defined by

$$V' = \{z \mid 0 < |z-1| < 1\}, \quad V = \{z \mid |z-1/2| < 1/2\}.$$

Then the analytic continuation of the element (V, f) of the function (19) from V to V' along any contour in V' homotopic to

$$\gamma_1 = \left\{ z \mid z = 1 + \frac{1}{2}e^{it}, \quad 0 \leq t \leq 2\pi \right\}$$

does not change the inner root sign because the point $z = 0$ is outside the contour. It only changes the sign of the outer root whenever the inner root sign is “−”. Indeed, representing $\sqrt{z} = \sqrt{1 + (z-1)} \simeq \left(1 + \frac{z-1}{2} - \frac{(z-1)^2}{8} + \frac{(z-1)^3}{16} \right)$, for $|z-1| \ll 1$, and using again the binomial expansion in V' we get

$$\sqrt{1 + \sqrt{z}} = \sqrt{2} \left(1 + \frac{z-1}{8} - \frac{5}{128}(z-1)^2 + \dots \right) \quad (\text{A.3})$$

$$\sqrt{1 - \sqrt{z}} = \frac{\sqrt{z-1}}{i\sqrt{2}} \left(1 - \frac{z-1}{8} + \frac{7}{128}(z-1)^2 + \dots \right), \quad z \in V'. \quad (\text{A.4})$$

The appearance of $\sqrt{z-1}$ in the right-hand side of Eq. (A.4) but not in Eq. (A.3) implies that when z encircles the point 1 the function $\sqrt{1 - \sqrt{z}}$ acquires one minus sign, while the function $\sqrt{1 + \sqrt{z}}$ is single-valued.

Recall that for a contour passing through the points $z = 0$ or $z = 1$ it is not possible to make analytic continuation.

Finally for $|z| > 1$ we use $W' = \{z \mid 1 < |z| < \infty\}$, $W = \{z \mid |z-2| < 1\}$, and the continuation along the contour

$$\gamma_2 = \left\{ z \mid z = 2e^{it}, \quad 0 \leq t \leq 2\pi \right\}$$

changes both the sign of the inner root and that of the outer root when the inner sign is “−”. Because in this case $|1/\sqrt{z}| < 1$ the binomial expansion with respect to $1/\sqrt{z}$ gives

$$\sqrt{1 \pm \sqrt{z}} = \sqrt[4]{z} \left(1 \pm \frac{1}{2\sqrt{z}} - \frac{1}{8z} \pm \frac{1}{16z\sqrt{z}} \dots \right), \quad 1 < |z| < \infty$$

and that explicitly shows that $z = \infty$ is a branching point of order 4.

That is how we conclude that the general contour γ , which is shown on Fig. A.1, corresponding to the read-out transformation (17) is homotopic to γ_0 or $\gamma_0 \cup \gamma_1$ depending on the value of $|x|$, i.e.,

$$\gamma \simeq \begin{cases} \gamma_0 & \text{for } |x| < 1 \\ \gamma_0 \cup \gamma_1 & \text{for } |x| > 1 \end{cases},$$

which explains once again the analytic continuation results obtained in Sect. 3.

References

- [1] F. Wilczek, *Fractional statistics and anyon superconductivity*. World Scientific, Singapore, 1990.
- [2] J. S. Birman, *Braids, Links and Mapping Class Groups*. Princeton Univ. Press, Ann. of Math. Studies, 82 ed., 1974.
- [3] K. Fredenhagen, K. H. Rehren, and B. Schroer, “Superselection sectors with braid group statistics and exchange algebras,” *Commun. Math. Phys.* **125** (1989) 201.
- [4] J. Fröhlich and F. Gabbiani, “Braid statistics in local quantum theory,” *Rev. Math. Phys.* **2** (1990) 251.
- [5] K. Fredenhagen, M. R. Gaberdiel, and S. M. Rueger, “Scattering states of plektons (particles with braid group statistics) in 2 + 1 dimensional quantum field theory,” *Commun. Math. Phys.* **75** (1996) 319, [hep-th/9410115](#).
- [6] J. Eisenstein, K. Cooper, L. Pfeiffer, and K. West, “Insulating and fractional quantum Hall states in the first excited Landau level,” *Phys. Rev. Lett.* **88** (2002) 076801.
- [7] J. Xia, W. Pan, C. Vicente, E. Adams, N. Sullivan, H. Stormer, D. Tsui, L. Pfeiffer, K. Baldwin, and K. West, “Electron correlation in the second Landau level: a competition between many nearly degenerated quantum phases,” *Phys. Rev. Lett.* **93** (2004) 176809.

- [8] N. Read and D. Green, “Paired states of fermions in two dimensions with breaking of parity and time-reversal symmetries and the fractional quantum Hall effect,” *Phys. Rev.* **B61** (2000) 10267, [cond-mat/9906453](#).
- [9] D. Ivanov, “Non-Abelian statistics of half-quantum vortices in p-wave superconductors,” *Phys. Rev. Lett.* **86** (2001) 268.
- [10] R. Morf, “Transition from quantum Hall to compressible states in the second landau level: new light on the $\nu=5/2$ enigma,” *Phys. Rev. Lett.* **80** (1998) 1505, [cond-mat/9809024](#).
- [11] E. Rezayi and F. Haldane, “Incompressible paired Hall state, strip order and composite fermion liquid phase in half-filled Landau level,” *Phys. Rev. Lett.* **84** (2000) 4685, [cond-mat/9906137](#).
- [12] G. Moore and N. Read, “Nonabelions in the fractional quantum Hall effect,” *Nucl. Phys.* **B360** (1991) 362.
- [13] P. Di Francesco, P. Mathieu, and D. Sénéchal, *Conformal Field Theory*. Springer–Verlag, New York, 1997.
- [14] A. Cappelli, L. S. Georgiev, and I. T. Todorov, “A unified conformal field theory approach to paired quantum Hall states,” *Commun. Math. Phys.* **205** (1999) 657–689, preprint ESI-621 (1998); [hep-th/9810105](#).
- [15] de Picciotto, M. Reznikov, M. Meiblum, V. Umansky, G. Bunin, and D. Mahalu *Nature (London)* **389** (1997) 162.
- [16] A. Stern and B. I. Halperin, “Proposed experiments to probe the non-abelian $\nu = 5/2$ quantum Hall state,” *Phys. Rev. Lett.* **94** (2006) 016802, [cond-mat/0508447](#).
- [17] P. Bonderson, A. Kitaev, and K. Shtengel, “Detecting non-abelian statistics in the $\nu = 5/2$ fractional quantum Hall state,” *Phys. Rev. Lett.* **96** (2006) 016803, [cond-mat/0508616](#).
- [18] L. S. Georgiev and M. R. Geller, “Aharonov–Bohm effect in the non-Abelian quantum Hall fluid,” *Phys. Rev. B* **73** (2006) 205310, [cond-mat/0511236](#).
- [19] D. E. Feldman and A. Kitaev, “Detecting non-Abelian statistics with electronic Mach–Zehnder interferometer,” (2006) [cond-mat/0607541](#).
- [20] P. Bonderson, K. Shtengel, and J. K. Slingerland, “Probing non-abelian statistics with two-particle interferometry,” (2006) [cond-mat/0601242](#).
- [21] S. B. Chung and M. Stone, “Proposal for reading out anyon qubits in non-abelian $\nu = 12/5$ quantum Hall state,” *Phys. Rev. B* **73** (2006) 245311, [cond-mat/0601594](#).
- [22] N. Read and E. Rezayi *Phys. Rev.* **B59** (1998) 8084.
- [23] A. Cappelli, L. S. Georgiev, and I. T. Todorov, “Parafermion Hall states from coset projections of abelian conformal theories,” *Nucl. Phys.* **B 599 [FS]** (2001) 499–530, [hep-th/0009229](#).

- [24] M. Nielsen and I. Chuang, *Quantum Computation and Quantum Information*. Cambridge University Press, 2000.
- [25] A. Kitaev, “Fault-tolerant quantum computation by anyons,” *Ann. of Phys. (N.Y.)* **303** (2003) 2.
- [26] L. H. Kauffman and S. J. Lomonaco Jr., “Braiding operators are universal quantum gates,” *New J. Phys.* **6** (2004) 134, quant-ph/0401090.
- [27] J. Preskill, “Topological quantum computation,” *Lecture Notes for Physics 219* (2004) <http://www.theory.caltech.edu/~preskill/ph219>.
- [28] S. D. Sarma, M. Freedman, and C. Nayak, “Topologically-protected qubits from a possible non-abelian fractional quantum Hall state,” *Phys. Rev. Lett.* **94** (2005) 166802, cond-mat/0412343.
- [29] M. Freedman, C. Nayak, and K. Walker, “Towards universal topological quantum computation in the $v = 5/2$ fractional quantum Hall state,” (2005) cond-mat/0512066.
- [30] J. Fröhlich, U. M. Studer, and E. Thiran, “A classification of quantum Hall fluids,” *J. Stat. Phys.* **86** (1997) 821, cond-mat/9503113.
- [31] J. Fröhlich and C. King, “Two-dimensional conformal field theory and three-dimensional topology,” *Int. J. Mod. Phys. A* **4** (1996) 5321.
- [32] J. Fröhlich, B. Pedrini, C. Schweigert, and J. Walcher, “Universality in quantum Hall systems: Coset construction of incompressible states,” *J. Stat. Phys.* **103** (2001) 527, cond-mat/0002330.
- [33] L. S. Georgiev, “The $v = 5/2$ quantum Hall state revisited: spontaneous breaking of the chiral fermion parity and phase transition between abelian and non-abelian statistics,” *Nucl. Phys. B* **651** (2003) 331–360, hep-th/0108173.
- [34] Y. Zhang, L. H. Kauffman, and R. F. Werner, “Permutation and its partial transpose,” (2006) quant-ph/0606005.
- [35] H. Bombin and M. Martin-Delgado, “Topological quantum distillation,” (2006) quant-ph/0605138.
- [36] D. V. Averin and V. J. Goldman, “Quantum computation with quasiparticles of the fractional quantum Hall effect,” *Solid State Commun.* **121** (2002) 25, cond-mat/0110193.
- [37] J. Preskill, “Quantum information and computation,” *Lecture Notes for Physics 229* (1998) <http://www.theory.caltech.edu/~preskill/ph229>.
- [38] S. Bravyi and A. Kitaev, “Universal quantum computation with ideal Clifford gates and noisy ancillas,” *Phys. Rev. A* **71** (2005) 022316.
- [39] C. Nayak and F. Wilczek, “ $2n$ quasiholes states realize 2^{n-1} -dimensional spinor braiding statistics in paired quantum Hall states,” *Nucl. Phys. B* **479** (1996) 529, cond-mat/9605145.

- [40] A. Stern, F. von Oppen, and E. Mariani, “Geometric phases and quantum entanglement as building blocks for non-Abelian quasiparticle statistics,” *Phys. Rev. B* **70** (2004) 205338.
- [41] V. Goldman, “Quantum antidot as an electrometer: Observation of fractional charge,” *Physica E* **1** (1997) 15–20.
- [42] C. Nayak, “private communication,” (2005).
- [43] Y. Ji, Y. Chung, D. Sprinzak, M. Heiblum, D. Mahalu, and H. Shtrikman, “An electronic Mach–Zehnder interferometer,” *Nature* **422** (2003) 415.
- [44] B. J. Overbosch and F. A. Bais, “Inequivalent classes of interference experiments with non-Abelian anyons,” *Phys. Rev. A* **64** (2001) 062107.
- [45] P. Furlan, G. Sotkov, and I. Todorov, “Two-dimensional conformal quantum field theory,” *Riv. Nuovo Cim.* **Vol. 12, No. 6** (1989) 1.
- [46] L. S. Georgiev, “Topologically protected quantum gates for computation with non-Abelian anyons in the Pfaffian quantum Hall state,” *Phys. Rev. B* (2006) (in press), [cond-mat/0607125](#).
- [47] D. Deustch, A. Ekert, and R. Lupacchini, “Machines, logic and quantum physics,” (1999) [math.HO/9911150](#).
- [48] H. S. M. Coxeter and W. O. J. Moser, *Generators and Relations for Discrete Groups*. Springer–Verlag, Berlin, third ed., 1972.
- [49] M. Hamermesh, *Group theory and its application to physical problems*. Dover Books on Physics and Chemistry, 1989.
- [50] G. Butler, “Dimino’s algorithm,” *Lecture Notes in Comput. Sci.* **559** (1991) 13.
- [51] N. Read, “Non-Abelian braid statistics versus projective permutation statistics,” *J. Math. Phys.* **44** (2003) 558.
- [52] D. Aharonov, “A simple proof that Toffoli and Hadamard are quantum universal,” (2003) [quant-ph/0301040](#).
- [53] Y. Zhang, L. H. Kauffman, and M.-L. Ge, “Yang–baxterizations, universal quantum gates and hamiltonians,” *Quant. Inf. Proc.* **4** (2005) 159, [quant-ph/0502015](#).
- [54] D. Arnaudon, A. Chakrabarti, V. K. Dobrev, and S. G. Mihov, “Exotic bialgebra S03: Representations, baxterisation and applications,” *Ann. Henri Poincaré* (2006) (to appear), [math.QA/0601708](#).
- [55] W. Pan, J.-S. Xia, V. Shvarts, D. E. Adams, H. L. Störmer, D. C. Tsui, L. N. Pfeiffer, K. W. Baldwin, and K. W. West, “Exact quantization of the even-denominator fractional quantum Hall state at $\nu = 5/2$ Landau level filling factor,” *Phys. Rev. Lett.* **83** (1999) 3530, [cond-mat/9907356](#).
- [56] B. Shabat, *Introduction to Complex Analysis*. Nauka (in russion), Moskow, 1969.